Ionizing Radiation Effects on Image Sensors

Method on Evaluation from an Image Quality Perspective

Johan Fagerström
johan.fagerstroem@gmail.com

Department of Electrical and Information Technology
Lund University

ISEC Industrial Security AB

Examiner: Erik Larsson
Advisor: Lars Öhlin

June 3, 2016

Printed in Sweden
E-huset, Lund, 2016

Abstract

Surveillance cameras are vital in the nuclear power industry where the reactor equipment must constantly be kept under surveillance to maintain safety. Constant monitoring is however difficult due to the highly radioactive environment, which cause cameras to malfunction and eventually break. Malfunction typically manifests itself as quality degradation of the image from the cameras. Initially, temporal noise appears on the image, while after some time in operation the image can be so distorted that the camera no longer serves its purpose.

The image sensor, which exists in every electronic camera, is a key component as it converts the physical image (visible light) to an electronic image. As ionizing radiation and light have similar properties, image sensors are also sensitive to ionizing radiation.

Previous work has evaluated various physical effects that ionizing radiation has on image sensors. Common is that the effects are visible on the image sensors output and imply a substantial impact on image quality. However, the main problem with previous evaluations is the difficulty to value and compare the results in respect to image quality impact. For example, it is difficult to determine whether *glass browning* causes more quality impact than *dark current increase*.

To address these problems, in this thesis we propose a method that evaluates the effects purely from the perspective of image quality. Metrics developed in the area of image quality assessment are used for measuring the image quality degradation. The radiation impact on image sensors is thus evaluated and quantified in a way that is more comprehensive, and where the results are easier valued and easier compared. Using the proposed method, questions such as *"Are CCD sensors more radiation tolerant than CMOS sensors?"* can be answered in a new sense.

The method is demonstrated upon four Omnivision OV7949 image sensors. The sensors are irradiated up to 1600 Gy in a `TRIGA Mark II` nuclear research reactor while gathering raw data. After finished irradiation process, the data is analyzed and the quality degradation induced by ionizing radiation is assessed and expressed in relation to absorbed dose. The result is visualized as plotted graphs,

and three measurements are made: initial-, cumulative and total degradation. To show how the results can be utilized and how the results are easily compared, we make an example of determining the best performing image sensor among the four evaluated.

Keywords: image sensor, CMOS, OV7949, electronic camera, radiation effects, ionizing radiation, image quality assessment, radiation tolerance.

Foreword and Acknowledgements

It has been challenging and highly rewarding to write a thesis on a subject which to some extent may sound like physics. **ISEC Industrial Security**, the funding company of this thesis, quested for different perspective on existing matters. As I was offered the task, the perspective became a Computer Engineer's. It feels thoroughly good to have left the comfort zone and explored foreign fields. With basic scientific understanding and *will* to learn about other concepts, nothing is impossible.

I would like to express my great gratitude to my examiner and advisor, **Dr. Erik Larsson**, for his superb guidance and deep experience from research projects. His support has been invaluable in times of disorientation and confusion. Without his answers to my many first-thesis-questions, the process would certainly have been more difficult.

Sincere thanks are also dedicated to my next advisor, **Lars Öhlin** at **ISEC**, who helped defining the thesis' aim and has been a great source of motivation and support along the way. It has been a great pleasure to work with him and the other colleagues at the company during these intense, but truly good months.

I'm proud to acknowledge the fine collaboration with **Klemen Ambrožič** at the **Jožef Stefan Institute** in Slovenia, who conducted the irradiation test.

Finally, but perhaps most importantly, I would like to honor my passed away grandfather **Bengt Fagerström**. As a retired physics teacher, he always encouraged curiosity and education. During my childhood years he taught me electronics and supplied me with physics- and electrical lab equipment. This formed my deep interest in technology, which eventually paved the way to Lund University. It would be my deepest wish to have him by my side when publishing this paper.

Johan Fagerström, 2016

Table of Contents

List of Figures

List of Tables

Terminology

Image sensor A device responsible for converting an optical image to an electronic image.

Camera The word camera in its original form refers to a device able to project an optical image of a reflected scene. In this report, the word *camera* refers to an electrical camera, which is a device that produces an electrical image from the optical one.

A (electrical) camera employs an image sensor, optics and an output interface. Occasionally, control and signal processing features may also be part of the camera domain.

Cameras and their relative context to image sensors is described in Chapter 1 and in Appendix A.

CCD - Charge-Coupled Device An image sensor technology, described in Appendix A.

CMOS - Complimentary Metal-Oxide Semiconductor An integrated circuit technology. One common application is image sensors, of which three types exist:

- **PPS - Passive Pixel Sensor**
- **APS - Passive Pixel Sensor**
- **DPS - Digital Pixel Sensor**

CMOS image sensors are described in Appendix A.

PAL - Phase Alternating Line A colour video encoding system used in television systems.

Ethernet Network layer protocol defined in IEEE 802.3.

The test system As part of the experiment where the method is demonstrated, the test system is was designed and built to create the image series where image quality degradation occurs as radiation is being absorbed.

IOE - Imager of Evaluation Term referring to the object being evaluated by the proposed method.

Initial quality degradation Image quality degradation occurring at the moment of which irradiation commences. The severity depends on radiation dose rate.

Total quality degradation Image quality degradation depending on absorbed dose.

Cumulative quality degradation Total quality degradation excluding the initial degradation.

Quality graph Graph showing the degradation of image quality in relation to absorbed dose.

Chapter 1

Introduction

In effort to ease the reading of this report, this introductory chapter aims to provide a comprehensive overview of the thesis' background, scope, contribution and organisation.

Section 1.1 briefly describes the fundamental basics of the most common and usual types of ionizing radiation. A short presentation of the previous work within the related fields is presented in Section 1.2. To comprehend how image sensors are related to cameras, an introduction to this is given in Section 1.3. Thesis Scope and Contribution are presented in Section 1.4 and Section 1.5 respectively. The organization of the report is described in Section 1.6.

1.1 Ionizing radiation

This section provides a brief introduction to the theory of ionizing radiation. Most facts are summarized from Curtis' online lecture [Cur].

To begin with, ionizing radiation is defined. The definition is followed by a description of different radiation types, radiation sources and how radiation is quantified.

1.1.1 Definition of ionizing radiation

Briefly defined, ionizing radiation is radiation that is capable of removing electrons from an atom, thus creating an ion. Ionization should not be confused with excitation, which is a similar phenomenon where enough energy is transferred to an orbital electron to displace it further away from the nucleus.

Absorption of radiation occurs when the **energy** of radiation is transferred to the atoms of the media through which it is passing. Higher energy radiation of the same type will naturally penetrate longer into the media. The energy of radiation

is usually denoted in electron-volt (eV), often with the SI-prefixes Kilo or Mega (k, M).

1.1.2 Types

This section describes different types of ionizing radiation. There exist two types of ionizing radiation: particulate and electromagnetic, described in Section 1.1.2.1 and 1.1.2.2 respectively. Particulate radiations are subatomic particles that has a certain mass (and occasionally a charge, depending on the particle). Electromagnetic radiations do not have a mass and no charge. This introduction regards three types of particulate radiation: alpha, beta and neutrons, and two types of electromagnetic radiation: X- and gamma rays.

1.1.2.1 Common Particulate Radiation

Alpha particles are Helium nucleus (consisting of 2 neutrons and 2 protons = a mass of 4 AMU). Since the nucleus are free from orbiting electrons, their charge is +2. Alpha particles are easily shielded with a sheet of paper or even human skin.

Beta$^-$ particles are electrons ejected from nucleus. Charge is -1 and mass 0.00055 AMU. Their energy typically ranges from several keV to 5 MeV. Usually shielded with aluminum.

Beta$^+$ particles are similar to Beta- particles except from their charge which is +1, which is referred to as a positron. The positron will quickly react with an electron and emit two 0.51 MeV gamma rays according to equation of mass-energy equivalence ($E = mc^2$).

Neutrons are particles ejected from nucleus. Their charge is naturally 0 and mass 1 AMU. They are unstable and decay by Beta$^+$ and Beta$^-$ particles with a half-life of approximately 13 minutes. Neutrons are categorized as Slow and Fast depending on their energy (<10keV and >10keV respectively). They are shielded in stages: Fast speed neutrons are "slowed down" with a hydrogenous material (for example water or concrete). A "slowed down" neutron will emit the excess energy as secondary radiation (alpha, beta or gamma). In a secondary stage, the slow neutrons are captured with a shielding material (for example boron).

1.1.2.2 Common Electromagnetic Radiation

A *photon* is an elementary particle and the quantum of electromagnetic radiation.

X-rays are photons emitted from electron orbits. The emission occurs when an excited electron falls to a lower energy orbit.

Gamma rays are photons emitted from the nucleus as a result of radioactive decay.

Photons can cause ionization in three ways: The photoelectric effect, the Compton effect and electron-positron pair production. The photoelectric effect occurs at low energy levels (< 0.5 MeV) and results in an electron being ejected. The photoelectric effect is the physical phenomenon which enables the functionality of image sensors. The Compton effect occurs at medium energy levels (0.5 - 5 MeV) and results in and electron being ejected and a photon with longer wavelength being emitted. The electron-positron pair production occurs at high energy levels (> 1.02 MeV, usually > 5 MeV) and results in an electron and a positron being ejected. As stated above, the electron and the positron will react and yield gamma radiation.

1.1.3 Radiation sources

Radiation comes from two groups of sources: natural and man-made. Natural sources include solar radiation, external terrestrial radiation and radioactive decay. An example of a man-made source, where the radioactive decay has been utilized for heating, is **nuclear power reactors**.

1.1.4 Quantification

Ionizing radiation involves a large number of quantities and units. This thesis mainly concerns the quantification of *absorbed dose*. The absorbed dose is the quota of absorbed energy per mass unit and is measured in Gray (Gy). **1 Gray = 1 Joule/kg**. The rate of which the dose increases is referred to as the *dose rate*, e.g. **Gy/h**.

1.2 Related work

Work related to this thesis exist within the fields of **image sensors** (specifically radiation effects) and **image quality assessment**.

A great deal of effort has been made to evaluate and quantify the effects that ionizing radiation has on image sensors and their surrounding environment. Three important effects are *glass browning*, *dark current increase* and *radiation induced noise*. Glass browning has earlier been quantified by measuring the change of optical density [HSA93] [Bis70] [EDASE08]. Dark current increase have been quantified using different methods depending on context and pre-conditions [BD00]. One example is the measurement of current change per unit of area of an image sensor surface [EAF02] [BDMU03]. The radiation induced noise has been quantified through counting the affected pixels [GK12].

All effects have in common that they affect image output and thus imply substantial impact on image quality. However, the results are obscure regarding the

image quality impact. As an example, it is difficult to determine whether *dark current* affects image quality more than *glass browning*. Another issue is that previous evaluations have been performed separately and exclude each other's effects.

This thesis aims to encounter such issues and proposes a method on how to evaluate radiation impact purely from the perspective of image quality.

Assessing image quality can be performed using subjective- or objective approaches. Subjective assessment performed by many human subjects is considered accurate, but irreproducible, time-consuming, expensive and not performed in real time [HB12]. If performed with a low number of subjects, it may be inaccurate since people tend to different quality issues.

Contrary to subjective approaches, objective assessment relies on mathematics. Algorithms computing the image quality serve as **image quality metrics**. Image quality metrics are divided in three classes; *no-reference-*, *reduced reference* and *full-reference* metrics. Full-reference metrics determine the test image's quality by comparing it against a reference image.

Due to the drawbacks of subjective methods, much work has been conducted in recent years to develop objective image quality metrics that correlate with human perception [WBL02]. The method proposed in this thesis utilizes three already existing and well-established full-reference metrics to assess the quality degradation of image sensors output, as an effect induced by ionizing radiation.

1.3 Context of image sensors

Although this thesis mainly regards image sensors, it is necessary to understand the context of image sensors and their relation to their surrounding environment.

In its original sense, a camera is a device that projects an optical image of a reflected scene. If this image is saved in some way, a photography has been produced. The word *camera* originates from the Latin expression *camera obscura* (dark room), which refers to a simple camera design proposed by Chinese philosopher Mozi who lived between 470 and 390 BC [Ham81]. The camera design employs a light shielded box, featuring a small pinhole (the aperture) on one side. The light from the reflected scene passes through the hole and projects an image on the opposite side of the box, as depicted in Figure 1.1.

Electronic cameras are cameras that produce an electrical image output. The output signal is formatted and interfaced according to certain standards. Examples of analogue standards are Phase Alternating Line (PAL) and National Television Systems Committee (NTSC), while examples of digital standards are more exotic. In situations of digital standards, the *data* can, for example, be of raw format or of compressed formats such as Joint Photographic Experts Group (JPEG). Further on, the formatted data is sent over a communication interface, for example Universal Serial Bus (USB), Camera Serial Interface (CSI), or even the Internet

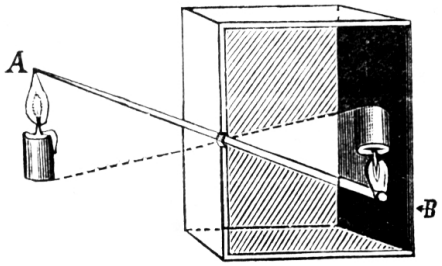

Figure 1.1: A *Camera Obscura*
[Dom10]

Protocol (IP) in situations of network cameras. From here and throughout this report, the term *camera* refers to *electronic camera*.

Every camera is equipped with an image sensor. The image sensor is responsible for converting the optical image (visible light, that is) to the electronic image mentioned above (see Appendix A for more information on image sensors and photo detection). To comprehend the context of the image sensor, a block diagram of an arbitrary camera is depicted in Figure 1.2. The block diagram describes the relation between image sensors and cameras. The image sensor is part of the camera domain. Control and signal processing elements are depicted on the image sensor borderline, which means that the elements reside in the camera domain, but may also be part of the image sensor. Putting such elements in the image sensor is becoming more usual as the CMOS manufacturing technology allows for easy integration [Fos97].

Additional components in the camera domain that are physically affected by radiation may as well introduce additional effects on image quality. To evaluate the radiation effects on *image sensors* only, it is therefore desirable to remove unnecessary components in the camera domain, and pursue an image sensor as bare as possible. On the other hand, pursuing a completely bare image sensor would not be sensible either. To evaluate image quality on meaningful pictures, some optics- and signal processing elements are required.

1.4 Thesis scope

The primary goal of this thesis is to propose a method on how to evaluate and quantify the effects that ionizing radiation has on image sensors. The method operates on image quality and utilizes three already existing and well-established image quality metrics for assessing quality degradation.

Within the scope of this thesis lies also to conduct an experiment to demonstrate the method. Due to the thesis time frame, we restrict ourselves to apply the method on one sensor model only. Four samples of the sensor are evaluated

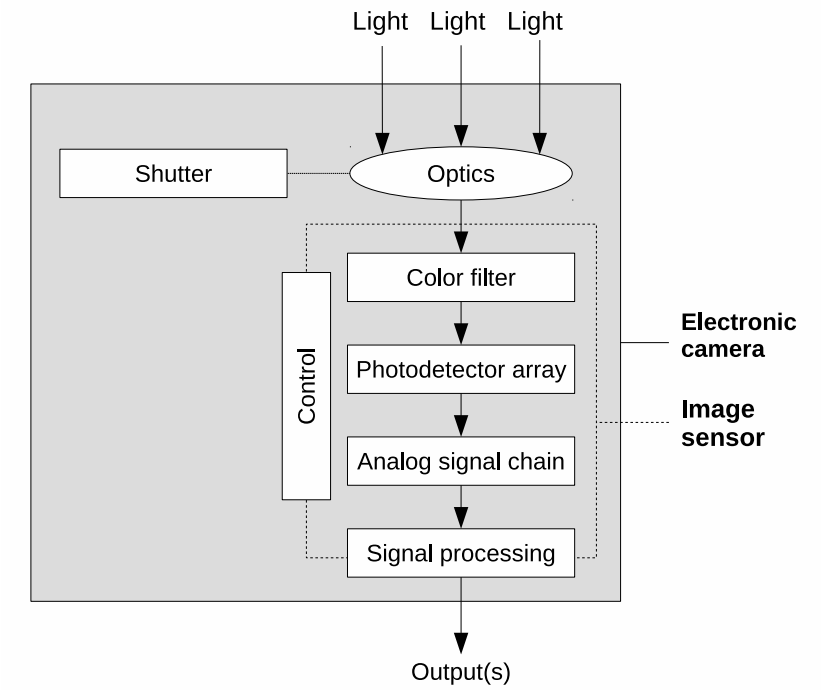

Figure 1.2: Functional block diagram of an arbitrary camera

due to possible batch deviation. The chosen sensor is the OmniVision OV7949, mounted in the Conrad RS-OV7949-1818 camera module. Putting the sensor in the context of a small camera module is necessary to produce meaningful experiment data.

In the demonstration experiment, we also restrict ourselves to use ordinary incandescent light as background lighting and let the camera modules reflect a scene of ordinary adhesive tape. Glass and polymers may be affected by ionizing radiation and introduce side effects captured by the proposed method. The irradiation test is restricted to 30 Gy/h of Gamma rays coming from a ^{235}U source.

1.5 Thesis contribution

This thesis contributes to the field of image sensors. Specifically, it introduces a novel method on how to evaluate and quantify the effects that ionizing radiation has on image sensors.

Previous work has been dedicated to evaluate various physical effects that ionizing has on image sensors. The effects have in common that they are visible on the image sensors output and imply a substantial impact on image quality. As

the effects are quantified in different manners it is difficult to compare the results of different effects in respect to image quality. For example, it is difficult to determine whether dark current increase causes more quality impact than radiation induced noise.

Contrary to previous work, the method proposed in this thesis evaluates the effects purely from the perspective of image quality. The radiation impact is thus quantified and measured in a way that is more comprehensive, easier valued and easier compared than previous quantifications.

Since the evaluated aspect is image quality, the evaluation method can be considered a black box test where the only input is images. The method is thus applicable to anything that produces images. This is desirable since there are different types, contexts and physical properties of image sensors.

As most evaluation methods consists of *observation* and *quantification*, so does the proposed method. The observation step is referred to as *data gathering*. Gathering data means to capture image series where quality degradation is visible as a result of absorbed dose. The second task is referred to as *analysis*, in which the image series are assessed in terms of already existing and well-established image quality metrics. Quantification is made using the units of the image quality metrics and Gray for absorbed dose. Three measures are defined from the results: initial-, cumulative and total degradation. The result is also visualized as plotted graphs.

1.6 Thesis organization

This thesis paper is divided in 6 chapters (including this one). Every chapter starts with a short introduction which briefly describes the chapter's content and aim. Chapters also end with a summarizing section, which concludes the chapter and introduces the next one. Chapter 2 describes three examples of effects that ionizing radiation has on image sensors. Discussed is how previous evaluations and quantifications of those effects do not suffice. Chapter 3 gives a detailed introduction to the image quality metrics utilized by the method to assess image quality. The metrics, their behavior and performance are discussed in respect to present research within the field of image quality assessment. Chapter 4 describes the proposed method on how to evaluate and quantify the effects that ionizing radiation induces on image sensors. In Chapter 5, the method is demonstrated in an experiment where the effects on the OV7949 sensor are evaluated. Finally, the conclusions drawn from this thesis and openings for future work is presented in Chapter 6.

Chapter 2

Previous Evaluations

This chapter provides an introduction to previous work on evaluating and quantifying the effects that ionizing radiation has on image sensors.

Section 2.1 describes three effects caused by ionizing radiation, and how these effects have previously been evaluated. The effects have in common that they are visible on the image sensors output and imply a substantial impact on image quality. Seen to the aspect of image quality, the previous evaluations and quantifications do not suffice. Why is motivated in Section 2.2.

2.1 Previous evaluations and quantifications

2.1.1 Glass browning

Browning is an effect on glass caused by ionizing radiation. As its name implies, glass turns to brown color (and sometimes other colors as well) as it is being irradiated [BN98] [HSA93].

Holmes-Siedle has performed an experiment which gives an example of glass browning influence in camera systems. In the experiment, a space television camera used for weather observation was evaluated. Its 10-component camera-lens system was irradiated to 1000 Gy. The result was a *"pronounced loss of transmission"*, whereas most of the lens elements turned straw yellow. Some even turned gray. Up to 50% recovery of performance occurred over a few months [HSA93].

ISEC Industrial Security has performed an unpublished experiment in which a 5 cm thick piece of PMMA acrylic glass was irradiated to 4000 Gy. The result is visible in Figure 2.1, where the irradiated piece is located to the left and a non-irradiated piece is located to the right.

A common quantification of effects in glass is to measure the change of optical density in relation to photon energy. The change of optical density naturally

varies between different glass materials [HSA93] [Bis70] [EDASE08].

In an experiment performed by El-Deen et al, quantification is also performed based upon the change of cut-off wavelength in relation to absorbed gamma dose [EDASE08].

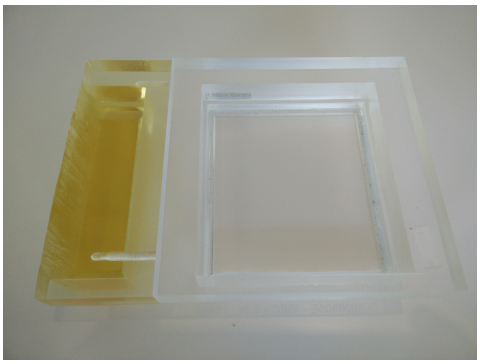

Figure 2.1: Glass browning in PMMA acrylic glass after 4000 Gy

2.1.2 Dark current increase

Dark current is the physical phenomenon of a photocurrent flowing through a photodetector even when the photodetector is not exposed to light. The dark current increases if the photodetector is being exposed to ionizing radiation. In the context of image sensors, the effect may emerge as a brighter image output with lower contrast. If some of the sensor's photodetectors are more affected than others, the result may emerge in the form of a fixed pattern noise.

In situations of stand alone photodiodes, the dark current effect has been evaluated numerous times. Bogaert et al. evaluated the effect on six different 5V biased diodes put under irradiation using a ^{60}Co source. Their quantification was performed by measuring the percentage of current increase in relation to total ionizing dose [BD00].

For CMOS APS image sensors, this has been evaluated by Eid et al [EAF02]. They quantify the effects by measuring the dark current intensity (pA/cm^2) in relation to total ionizing dose. A similar evaluation and quantification was performed by Bogaerts et al [BDMU03].

Dark current increase in CMOS APS sensors has also been evaluated by Gumiela et al. Their approach was to measure the quotient $V/Vmax$ for each pixel in relation to time. The observation was performed while the image sensor was irradiated with alpha particles from an ^{241}Am source.

Hopkinson has evaluated the dark current increase of an 512×512 image sensor manufactured by IMEC. Irradiation was performed with 10 MeV protons. The sensor was split in three regions, whereas two of them were irradiated with 2

kRd and 4 kRd respectively [H$^+$00]. After irradiation, the image captured by the image sensor is shown in Figure 2.2.

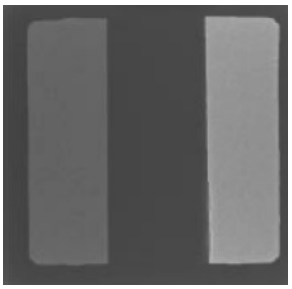

Figure 2.2: Dark current effect on an image sensor [H$^+$00]

2.1.3 Radiation induced noise

Ionizing radiation causes noise on image sensors output. Two major sources of radiation induced noise exist:

- Dark current increase of individual pixels, yielding a fixed-pattern noise.
- Inducing photocurrent in individual pixels by incident particle interaction, Compton- or photoelectric effect. The interaction is similar to ordinary photodetection [HSA93]. The emerging noise is temporal.

Attempts have been done to quantify these effects. Gumiela et al evaluated the effects on a CMOS APS sensor. Quantification was performed by measuring the count of affected pixels per second in relation to dose rate (mGy/h) [GK12]. For a CCD sensor, Gumiela et al quantified the effects by counting the affected pixels of a number of images taken under irradiation of alpha particles from a ^{241}Am 33 kBq source [GK12].

2.2 Discussion

When comparing performance of imaging devices it is natural to consider image quality. In consideration of image quality, the above quantifications are obscure and may not be easily valued or compared. For an example, it is difficult to determine whether glass browning disturbs image quality more than dark current increase.

The above described evaluations also have a common drawback: they are performed separately and exclude each other's effects. Whereas all of them have

Figure 2.3: Radiation induced noise

impact on image quality, evaluating ionizing radiation effects from the perspective of image quality would thus include all of the above effects.

Dark current increase is normally evaluated in a completely light-shielded environment [BDMU03] [EAF02]. Such an environment does not provide meaningful input in respect to image quality, as image sensors most often depict something visible. An evaluation method operating on image quality would allow meaningful input, since anything can be depicted when comparing image quality.

Quantifications depending on certain hardware involves complications. For example, different image sensors may use different types of glass - both in the chip window and in the surrounding optics. Which type of glass is normally not specified in image sensor data sheets, hence the measurement of optical density change is a problematic quantification when comparing image sensors' radiation performance. Evaluating radiation effects from the black-box perspective of image quality would not depend on certain hardware as all image sensors produce images.

2.3 Chapter summary

This chapter has reviewed three effects that ionizing radiation has on image sensors and their surrounding environment. The effects have in common that they are visible image sensors' output.

Previous work within the field has made effort to evaluate and quantify these effects separately, and not in consideration to image quality. As argued in the dis-

cussion section, evaluating radiation effects from the perspective of image quality holds several advantages.

In the next chapter, three metrics from the field of image quality assessment are described.

Chapter 3

Image Quality Metrics

A lot of work has previously been done within the field of objective image quality assessment. In the continuous pursuit of metrics that resembles the perception of the human visual system, metrics are invented and improved all the time. This chapter provides an introduction to three full-reference metrics and their operation.

The metrics are:

- **Peak Signal to Noise Ratio (PSNR)**, described in Section 3.1.
- **Structural Similarity Index (SSIM)**, described in Section 3.2
- **Improved CIELAB (ΔIE)**, described in Section 3.3.

3.1 Peak Signal to Noise Ratio

Peak Signal to Noise Ratio (PSNR) is the ratio of the maximum possible power of a signal and the power of the corrupting noise. PSNR is a full-reference metric originating from the field of signal processing. In context of image quality assessment, the *signal* constitutes of the reference image and the *noise* refers to the assessed image.

PSNR is calculated from the Mean Squared Error (MSE). The MSE is literally described as iterating through both entire images, calculating the color difference (the *error*) for each pixel. To get rid of negative values, the difference is squared. Finally, the mean of the squared differences is calculated, hence *Mean Squared Error*. The MSE is defined in Formula 3.1 [Mat16d] [Mat16c] [HZ10].

$$MSE = \frac{1}{mn} \sum_{i=0}^{m-1} \sum_{j=0}^{n-1} [Ref(i,j) - A(i,j)]^2 \tag{3.1}$$

where *Ref* is the reference image, A is the assessed image, m and n are the image dimensions.

Due to wide dynamic range of signals, PSNR is expressed in logarithmic decibel scale, see Formula 3.2. MAX_{Ref} is the dynamic range of the signals. For an image with 8-bit pixel color representation the dynamic range is $2^8 - 1 = 255$.

$$\begin{aligned} PSNR &= 10\log_{10}\left(\frac{MAX_{Ref}^2}{MSE}\right) \\ &= 20\log_{10}\left(\frac{MAX_{Ref}}{\sqrt{MSE}}\right) \\ &= 20\log_{10}\left(MAX_{Ref}\right) - 10\log_{10}\left(MSE\right) \end{aligned} \tag{3.2}$$

For color images, MSE is calculated as the average of each color layer's MSE. For example; in an RGB image, the layers are the red, green and blue values. The example of an RGB image's MSE is defined in Formula 3.3.

$$MSE_{RGB} = \frac{MSE_R + MSE_G + MSE_B}{3} \tag{3.3}$$

Formula 3.2 satisfies the following conditions:

- Symmetry: $PSNR(x, y) = PSNR(y, x)$
- Bounds: $PSNR(x, y) \geq 0dB$
- No max value: $PSNR(x, y) \rightarrow infinity$ when $x \rightarrow y$

3.2 Structural Similarity Index

Under the assumption that the perception of the human visual system is highly sensitive to structure of images, Wang et al. proposed a metric for quality assessment based on difference in structure. *Structural Similarity Index* (SSIM) has proved being more accordant to human visual perception than, for example, PSNR [WBSS04].

SSIM operates only on grayscale images. RGB images must therefore be converted to grayscale. This is commonly done by combining the RGB values into luminance using a weighted mean, for example, the rgb2gray-function in the Matlab Image Processing Toolbox [Mat16a]. The weights are denoted in Formula 3.4.

$$Luminance = 0.2989 * R + 0.5870 * G + 0.1140 * B \tag{3.4}$$

The SSIM function is divided in three components. The components measure luminance, contrast and structure, as described by Formula 3.5. x and y are the reference- and the assessed images.

$$\begin{aligned} \text{l(x,y)} &= \frac{2\mu_x\mu_y + C_1}{\mu_x^2 + \mu_y^2 + C_1} \\ \text{c(x,y)} &= \frac{2\sigma_x\sigma_y + C_2}{\sigma_x^2 + \sigma_y^2 + C_2} \\ \text{s(x,y)} &= \frac{\sigma_{xy} + C_3}{\sigma_x\sigma_y + C_3} \end{aligned} \tag{3.5}$$

- μ_x is the mean of x
- σ_x^2 is the variance of x
- σ_{xy} is covariance of x and y

The statistics are calculated locally within a statistics window that is moved iteratively over the image. The window differs between implementations. In the Matlab Toolbox and in the Wang et al. implementation, the default setting is a 11×11 Gaussian weighting function with standard deviation 1.5. Certain implementations allow the window to be adjusted through parameters [Mat16e] [WBSS04]. C_1, C_2 and C_3 are constants (that stabilizes the fractions) given by

$$\begin{aligned} C_1 &= (K_1 L)^2 \\ C_2 &= (K_2 L)^2 \\ C_3 &= C_2/2 \end{aligned} \tag{3.6}$$

L denotes the dynamic range of the signals. K_1 and K_2 is generally set to 0.01 and 0.03 respectively [WSB03] [Mat16e].

The components are combined by multiplication as described by Formula 3.7.

$$\text{SSIM(x,y)} = [l(x,y)]^\alpha \cdot [c(x,y)]^\beta \cdot [s(x,y)]^\gamma \tag{3.7}$$

where α, β and γ are parameters to define the relative importance of the three components. Setting the parameters $\alpha = \beta = \gamma = 1$ yields Formula 3.8.

$$\text{SSIM(x,y)} = \frac{(2\mu_x\mu_y + C_1)(2\sigma_{xy} + C_2)}{(\mu_x^2 + \mu_y^2 + C_1)(\sigma_x^2 + \sigma_y^2 + C_2)} \tag{3.8}$$

Formula 3.8 satisfies the following conditions:

- Symmetry: $SSIM(x,y) = SSIM(y,x)$
- Bounds: $0 \leq SSIM(x,y) \leq 1$

- Unique max value: $SSIM(x, y) = 1$ if and only if $x = y$

SSIM has the possibility to be adjusted through its parameters (α, β, γ, K_1, K_2, and the statistics window).

3.3 Improved CIELAB

Relying on calculations similar to the MSE (Formula 3.1), Hassan proposed in 2015 the *Improved CIELAB* metric (abbreviated ΔIE). As its name implies, the metric operates in CIELAB color space [Has15]. The metric algorithm utilizes a Just-Noticable-Color-Difference (JNCD) threshold, which in CIELAB has been determined to 2.3 by Mahy et al. in 1994 [MEO94].

The CIELAB 1976 is a three-dimensional (**L**, **a** and **b**) color space, where the L dimension represents a lightness scale and the a- vs. b dimensions represent opponent color scales. Colors are thus represented as 3D points.

The difference between two colors in CIELAB color space is calculated as the Euclidean distance, referred to as dE or ΔE.

$$\Delta E = \sqrt{(\Delta L)^2 + (\Delta a)^2 + (\Delta b)^2} \tag{3.9}$$

The metric, as proposed by Hassan, calculates the mean value of all pixels' dE (whereas one pixel is from the reference image and one from the assessed image). If the dE for one pixel is below **2.3** (the JNCD threshold), that pixel is not accounted for in the mean value. The algorithm is denoted in Formula 3.10, where ΔIE is the metric value, Ref is the reference image, A is the assessed image, $d[]$ is the Euclidean distance between the two pixels in CIELAB and m, n are image dimensions.

$$\begin{aligned} \Delta IE &= \frac{1}{mn} \sum_{i=0}^{m-1} \sum_{j=0}^{n-1} d[Ref(i,j),\, A(i,j)]\delta_{ij} \\ \delta_{ij} &= \begin{cases} 1 \text{ if } d[Ref(i,j),\, A(i,j)] > JNCD_{CIELAB} \\ 0 \text{ otherwise} \end{cases} \end{aligned} \tag{3.10}$$

Formula 3.10 satisfies the following conditions:

- Symmetry: $\Delta IE(x, y) = \Delta IE(y, x)$
- Bounds: $\Delta IE(A, Ref) \geq 0$

3.4 Metrics' weaknesses and strengths

It is well concluded that the PSNR lacks correlation to the perception of the human visual system [Gir93] [MRLP+]. SSIM has been proved better correlated to the human visual system than PSNR [WBSS04]. For some quality factors, Improved CIELAB has been proved even better correlated than SSIM [Has15].

In an analysis, Horé et al. draw the conclusion that the PSNR is more sensitive to Gaussian noise than the SSIM. However, it is also revealed that both PSNR and SSIM are more sensitive to Gaussian noise than Gaussian blur [HZ10]. One of the key effects of ionizing radiation is noise, whereby it is important that metrics tend to noise as a quality factor.

SSIM has the major drawback that it only operates on grayscale images. When converting RGB to grayscale, the RGB values are combined using a weighted mean [Mat16a]. That implies quality factors in one layer may be reduced when converted to grayscale.

3.5 Chapter summary

This chapter has reviewed two classic metrics (PSNR and SSIM) and a recent one (ΔIE).

The next chapter describes how the above metrics are utilized in the proposed method, in which they serve to assess the image quality degradation induced as an effect of ionizing radiation exposure.

Chapter 4

Proposed Method

This chapter describes the proposed method on how to evaluate the effects that ionizing radiation causes on image sensors. The method evaluates the effects purely from the perspective of image quality, thus encountering the issues with previous evaluations of radiation effects. The image quality metrics described in Chapter 3 are used for measuring the image quality degradation.

As most evaluation methods consist of *observation* and *quantification*, so does the proposed method. However, for clarity, we refer to them as *data gathering* and *analysis*:

1. **Data gathering:** Creating image series, where image snapshots are captured periodically over time whilst the IOE is being irradiated.
2. **Analysis:** Quality assessing the image series. The result expresses the image quality degradation in relation to absorbed dose. Three measures of quality degradation are defined: total-, initial- and cumulative degradation.

The two steps are described in Section 4.2 and Section 4.3 respectively. To implement the method, a test environment is required. The test environment requirements are specified in Section 4.1.

4.1 Test environment requirements

Executing the method requires a test environment. The test environment must consist of an active space and a non-active space. The spaces must be divided by a barrier that also can be crossed by running cables. The desire for the two spaces and the dividing barrier is to provide a safe place for the data storage and the control equipment that issues the image snapshots.

The test environment must include a dosimeter which logs the values of absorbed dose. The dose values are later used to express the quality degradation in relation to absorbed dose.

It is also desired, but not required, that the test environment is capable of maintaining a constant dose rate in order to avoid effects caused by dose rate changes.

An abstract model of how the test environment must be organized is depicted in Figure 4.1.

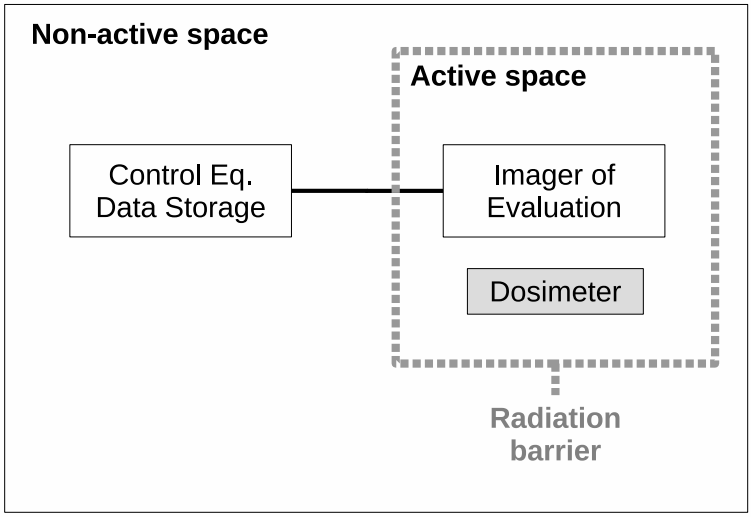

Figure 4.1: Test environment: Abstract model

Example: A `TRIGA Mark II` nuclear research reactor meets the requirements for test environment.

4.2 Data gathering

To gather the data needed for evaluation, a series of images has to be created. The purpose of the image series is to capture the ionizing radiation induced effects on image output.

The control equipment (outside the radiation barrier) issues and stores the actual image snapshots, using the IOE. The images are taken periodically (described by flowchart in in Figure 4.2) while the IOE is being exposed to ionizing radiation. The period time determines the amount of images taken, which further on determines the precision of the evaluation. The period time is not specifically prescribed by the method since it depends on the irradiation dose rate and total

dose tolerance of the IOE. This has to be estimated, or decided through empirical studies.

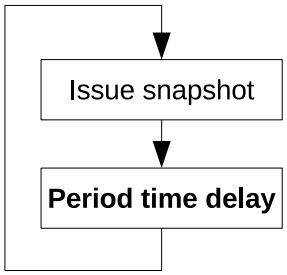

Figure 4.2: Capture sequence

Below is a list of crucial details:

- To take the initial quality degradation into account (that is the degradation occurring at the very moment at which irradiation commences), the capture of images must start before irradiation.
- The scene reflected by the cameras must not alter since that will affect the image quality. That implies that the scene (including background lighting) must be of radiation hard materials. That means also that the IOE must remain mechanically in the same position relative to the reflected scene.

4.2.1 Optional

The options in the list below provide additional feedback and information, but are not mandatory.

- If desired to perform evaluation on realistic input images, it is necessary to put the image sensor in context of a simple camera featuring lighter optics.
- The IOE *should* be irradiated with a constant dose rate in order to avoid effects caused by dose rate changes.
- In order to provide the IOE with an image that tests all of the photo detectors of the imaging array (see Section A.3 for information on color filtering), the IOE should reflect a multi-colored scene.
- In order to distinguish that the IOE has not frozen (that it does not continuously send the same picture), an active object can be put in the reflected scene. The active object can, for example, be a flickering LED. If this is done, two images should be taken correspondingly - one with the LED off and one with the LED on. The analysis is then performed on one of those. Note that the capture sequence will then be different from the sequence depicted in Figure 4.2.

4.3 Analysis

In the analysis step, the image quality degradation of the image series is assessed and quantified using the metrics specifically described in Chapter 3. The degradation is expressed in relation to absorbed dose which is measured in Gray (Gy).

As the quality metrics are only capable of assessing individual images, the image series has to be looped through and each image's quality individually assessed. Pseudo-code Algorithm 1 describes how this is performed. *qualityMetric(..)* refers to one of the utilized quality metrics. The procedure is repeated for all of the quality metrics.

In the end of Algorithm 1, the quality values are plotted in relation to corresponding values of absorbed dose. The graph is referred to as a *quality graph* and visualizes the *total degradation* (see list below). Figure 4.3 shows an example of an PSNR quality graph yielded from Algorithm 1.

Three different measures of quality degradation can be defined from the quality- and dose values. The measures are listed and described below. Examples of results are shown in Table 4.1, using the same source as the quality graph in Figure 4.3.

- The *total degradation*, as plotted in the graphs.
- The *initial degradation*, occurring as irradiation commences. At that moment, the IOE has not been exposed to radiation for any time. The severity of initial degradation does therefore depend on radiation dose rate, rather than the dose itself.
- The *cumulative degradation*, occurring while being exposed to radiation. The cumulative degradation excludes the initial degradation and is only a measurement of the quality degradation occurring after the initial degradation. The cumulative degradation is calculated as described by Formula 4.1 and 4.2.

$$Cumulative = Initial - Total \tag{4.1}$$

$$Cumulative = Total - Initial \tag{4.2}$$

  Two formulas are needed as some metrics (PSNR, SSIM) considers high values as better, whereas some metrics (Improved CIELAB) considers high values as worse. Formula 4.1 is used for PSNR and SSIM, Formula 4.2 is used for Improved CIELAB.

Algorithm 1: Quality assessing image series

Data: The image series.
Result: Quality- and dose values. A graph displaying the *total quality degradation* in relation to absorbed dose.

```
image ref = <the first image of the series>;
double[] metricValues;
double[] doseValues;
integer i = 0;
for every image img do
    metricValues[i] = qualityMetric(ref, img);
    doseValues[i] = getDose(img);
    i++;
end
plot(doseValues, metricValues);
```

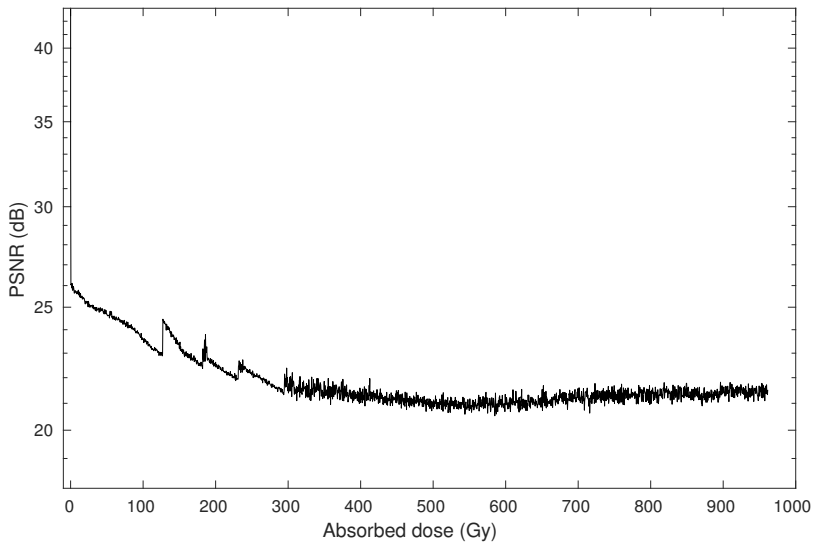

Figure 4.3: An example of a PSNR quality graph

Initial degradation	26 dB
Total degradation by 500 Gy	21 dB
Cumulative degradation by 500 Gy	5 dB

Table 4.1: Example results (same source as Figure 4.3)

4.4 Chapter summary

This chapter has described the proposed method on how to evaluate and quantify the effects that ionizing radiation causes on image sensors.

The method operates from the perspective of image quality, thus including the previously known effects described in Chapter 2. The method also solves the problem of hardware dependence, as all image sensors produce images. The method can be considered a black box test, where the only input is electronic images. This enables possibilities to answer questions such as *"Are CCD sensors more radiation tolerant than CMOS sensors?"* in a new sense than before.

The next chapter describes and demonstrates an implementation of the proposed method.

Chapter 5

Experiment

This chapter describes the experiment conducted to demonstrate the proposed evaluation method.

Section 5.1 presents the image sensor used as evaluation object and its application in a small camera module. Having the sensor in the context of a camera module is necessary to receive meaningful data. Due to possible deviations of radiation tolerance between component batches, four samples of the module are evaluated. Section 5.2 describes how the data gathering was performed. This includes an introduction to the test environment, how the irradiation was performed and how the image series was created. Section 5.3 presents the analysis and the results. The complete evaluation is summarized in Section 5.4.

5.1 The IOE

The *OmniVision OV7949* CMOS PPS image sensor is used as evaluation object. The sensor is present in the context of a small camera module, the *Conrad RS-OV7949-1818* [Con][Omn09].

The OV7949 sensor was mainly chosen with reason of its PAL signal output, which can be transferred over long distances without severe complications. This is required by the test environment, see Section 5.2.1.

The camera module includes a wide-angle lens, a 6206A voltage regulator and a number of resistors. Beyond the image sensor and the voltage regulator, no additional semi-conductor components are present in the camera domain. The OV7949 sensor itself features several embedded signal processing- and control features, such as the PAL encoding, auto white balance, aperture and gamma correction [Omn09].

Figure 5.1: Conrad RS-OV7949-1818: Camera module [Con]

5.2 Data gathering

To create the image series, in which the quality degrades in relation to absorbed dose, the RS-OV7949-1818 camera modules were exposed to gamma radiation until they were completely out of operation. Whilst being irradiated, they continuously sent live PAL video picturing the test scene. To capture the series of still pictures from the camera modules' video output, a *test system* was constructed.

This section describes how the above was realised, including the test system's design and functionality. The description also includes the test environment in which the system was deployed and utilized, and how the irradiation was performed.

5.2.1 Test environment

The irradiation was conducted in a `TRIGA Mark II` nuclear research reactor at the *Jožef Stefan Institute* in Slovenia.

Effort was put into maintaining a constant dose rate of **30 Gy/h**. 30 Gy/h was the highest dose rate that the reactor could maintain on a relatively constant level. Due to specific circumstances of the test environment, the dose rate decreased marginally over time, yielding the statistics in Table 5.1

Initial dose rate	29.7 Gy/h
Closing dose rate	22.7 Gy/h
Mean value	24.0 Gy/h
Standard deviation	1.49 Gy/h

Table 5.1: Dose rate statistics

In order to make a distinguishable start of quality degradation, the capture process commenced before the irradiation.

5.2.2 Test system

To capture the series of images, a test system was designed specifically for the test environment. The test system was developed in two modules referred to as the *inside reactor module* and the *outside reactor module*.

The test system's physical topology, in which the two modules are highlighted, is depicted in Figure 5.2.

5.2.2.1 Inside reactor module

As stated, the test system employs four RS-OV7949-1818 camera modules. The cameras modules are mounted on an aluminum construction together with background lighting (incandescent light bulbs).

The camera modules are mounted in a 2×2 matrix. The light bulbs (background lighting) is symmetrically mounted side by side of the matrix. Symmetry is desired with reasons of shielding. One camera module must not be more shielded from radiation than another, and one camera module most not be exposed to more light than another. The camera module matrix mount, arranged together with the background lighting, is depicted in Figure 5.3.

The camera modules reflect a surface that is covered with adhesive tape in different colors; white, yellow, red, green and blue. The different colors provides the image sensor with an image that activates all of the photodetectors (see A.3 for information on color filtering).

In the centre of the above mentioned surface, an LED is mounted. To see if any of the camera modules have frozen (sending the same picture), a pair of images are taken correspondingly in each iteration – one normal snapshot, and one with the LED lit up. The capture sequence is specified in Figure 5.8.

The inside reactor module is depicted in Figure 5.4.

5.2.2.2 Outside reactor module

To convert the PAL signals from the camera modules, an Axis M7014 video encoder was used. The encoder is interfaced through IP/Ethernet, over which it's able to stream video and capture still pictures.

The LED (introduced above) is controlled by a Velleman VM204 I/O module, which is also interfaced through IP/Ethernet.

The M7014 video encoder and the VM204 I/O module were chosen with reason of their platform independence - almost every workstation computer, as of year 2016, features at least one Ethernet NIC.

The M7014 and the VM204 was built into a plastic enclosure. The entire assembly is referred to as the *outside reactor module*.

Additionally, an Ethernet switch was built into the module. The switch connects the M7014 and the VM204 with the network of the control platform workstation.

For simplicity, power supplies that power both the inside and the outside modules were also placed in the outside reactor module. For easy deployment, the module was equipped with standard connectors (RJ-45 for Ethernet, BNC for video, power cord and a control cable).

The outside reactor module is depicted in the photo of Figure 5.5, whereas the entire system is depicted in Figure 5.6.

5.2.2.3 Capture software

To put the above described hardware modules in operation, an application was executed on the control platform workstation (connected to the outside reactor module). The application was developed in **Java SE 1.7**.

The applications primary objective is to issue the image snapshots and save them in JPEG-format. While running, the application logs the occurring events for possible post analysis.

The application interfaces the hardware (the M7014 and the VM204) using RESTful API's over HTTP. Feedback is received as HTTP response codes and as JSON formatted content [Axi13][Vel16].

For reasons of usability, the application features a graphical user interface developed using the Swing- and AWT frameworks. The GUI consists primarily of one main window. In the main window, the last snapshot pairs and controls for starting and stopping capture is available. A screenshot of the main window is shown in Figure 5.7.

5.2.2.4 Capture sequence

As the method prescribes, the images of the series' are taken periodically with a period time delay in the end of each iteration. With experience from earlier experiments, the delay was determined to 60+5 seconds (5s LED rise time, see motivation below). Reckoning that the sensor will withstand an absorbed dose of 300 Gy, it will remain functional for 10 hours when being irradiated with 30 Gy/h. Performing an iteration every 60 seconds for 10 hours equals 553 iterations, thus 553 images per camera module, which will suffice as resolution.

As stated above, the LED is used to see that the camera modules have not frozen. Since the image sensor features automatic white balance, gamma- and aperture correction, it is necessary to precede the LED's "duty cycle" with a rise time delay. A pro-experimental investigation was conducted to determine the delay, whereas

it was determined to **5 seconds**. Fall time delay is not necessary since the LED's duty cycle is followed by the interval delay. The capture sequence is denoted in Figure 5.8.

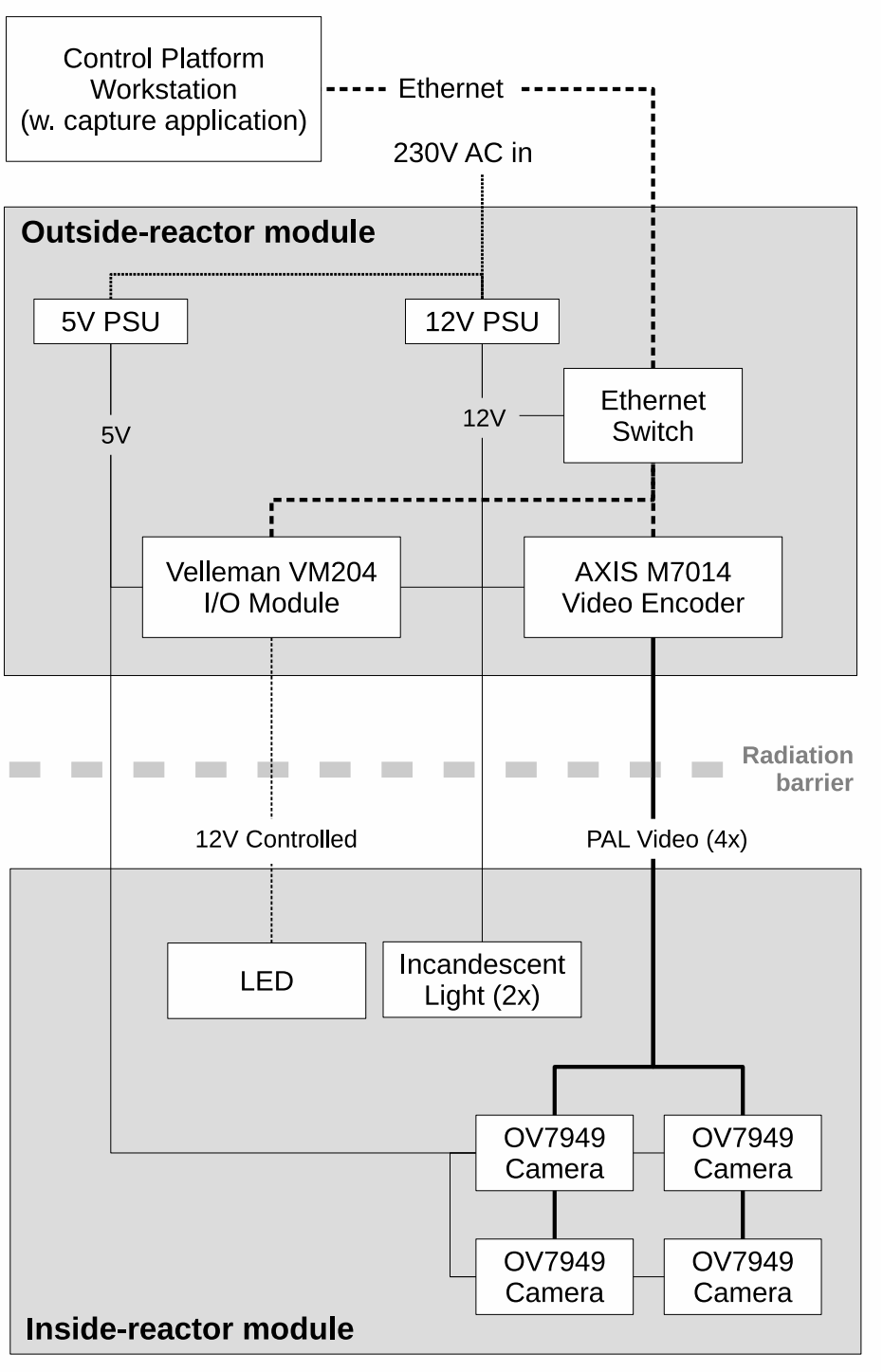

Figure 5.2: Test system: Physical topology

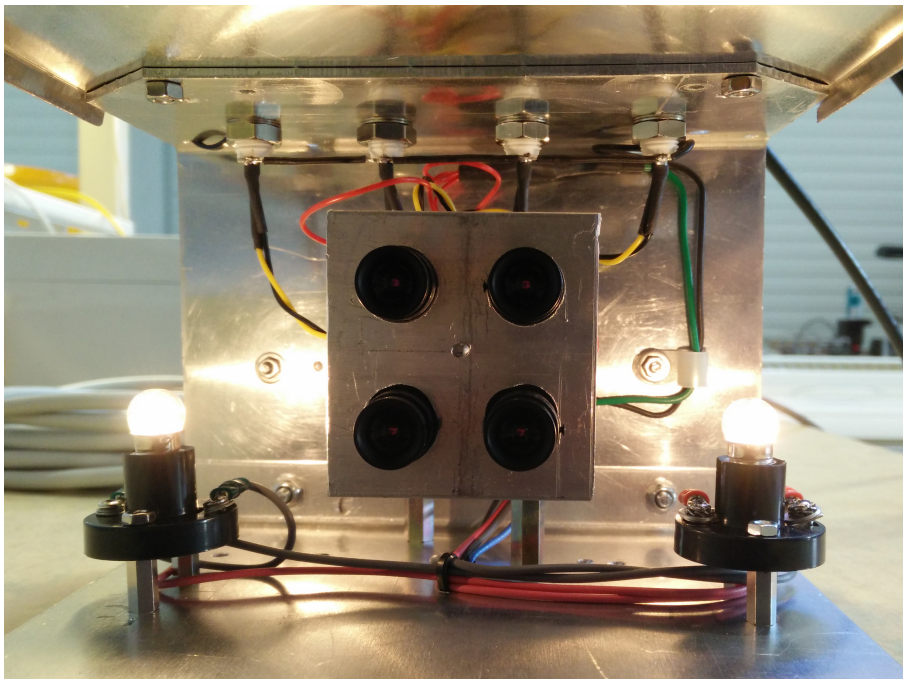

Figure 5.3: Inside reactor module: Camera matrix mount

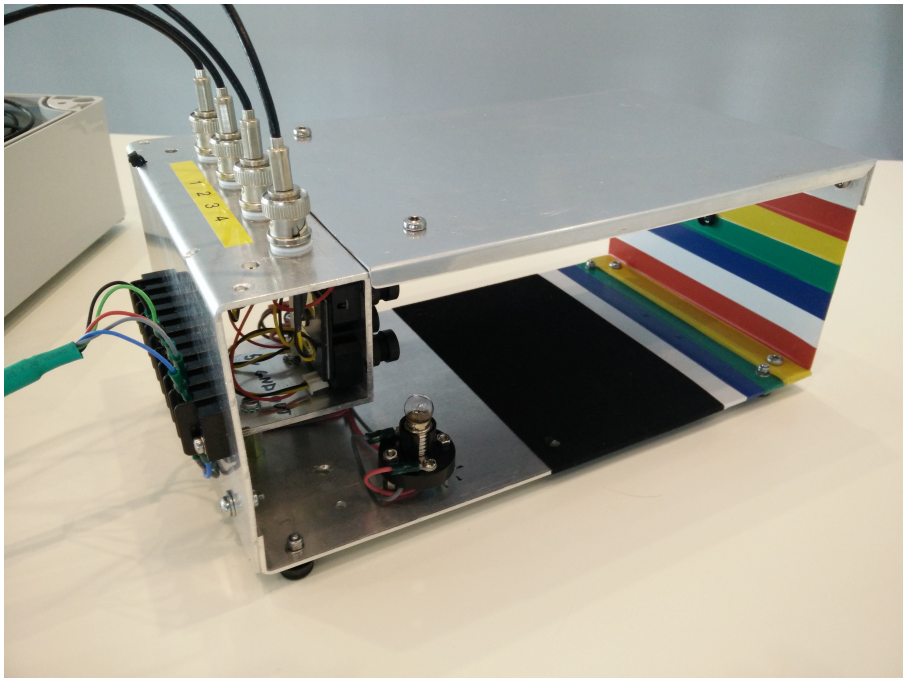

Figure 5.4: Test system: Inside reactor module

Figure 5.5: Test system: Outside reactor module

Figure 5.6: Overview of the entire test system

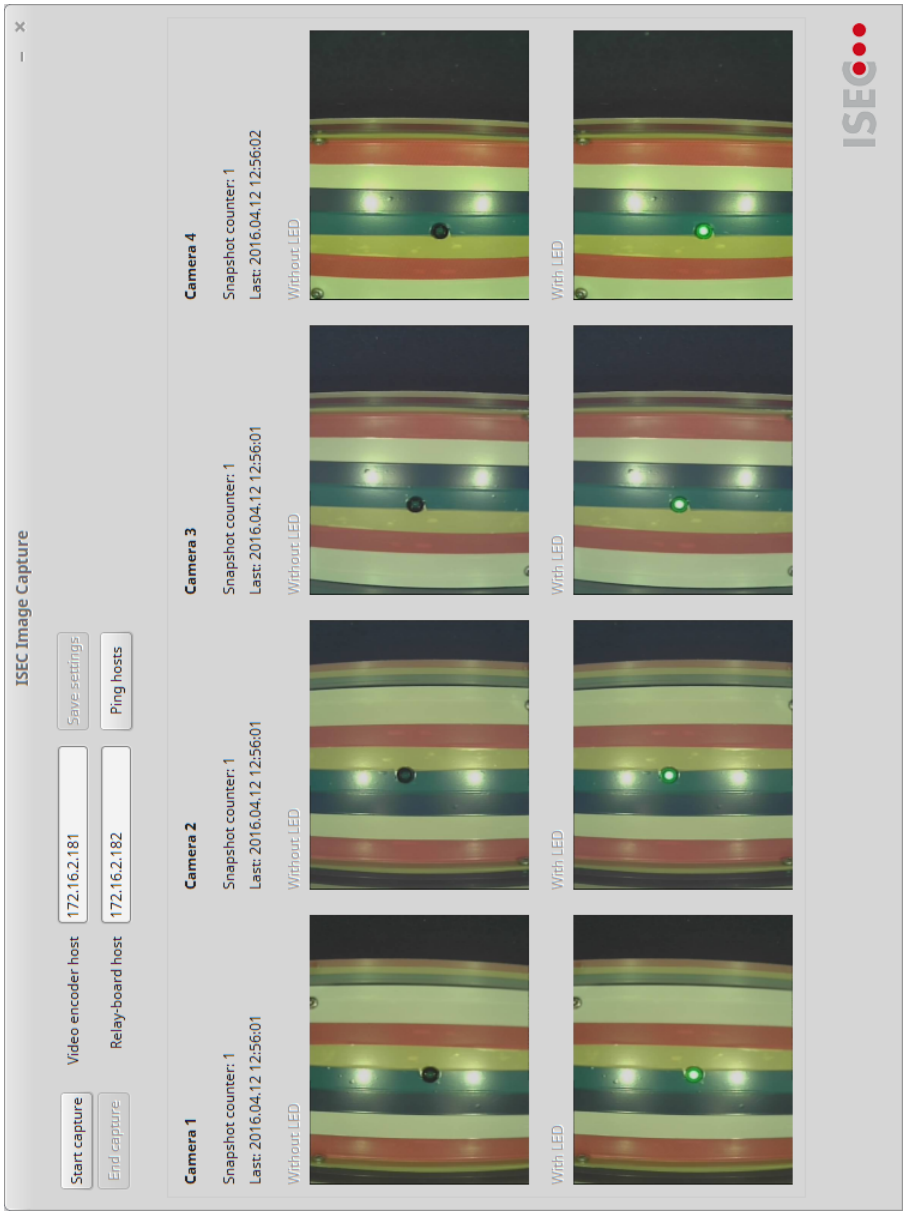

Figure 5.7: Test system: Capture application in GTK+

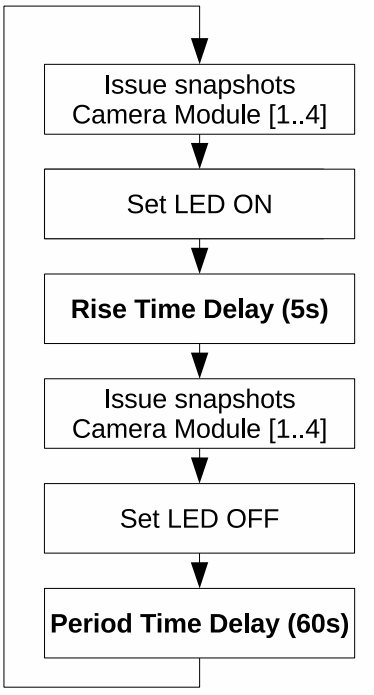

Figure 5.8: Capture sequence

5.3 Analysis and result

This section presents the analysis step of the evaluation, including a comprehensive presentation of the results. In Section 5.3.1, the results are discussed in respect to each image quality metric. Section 5.3.2 presents the quality graphs for each metric and camera module. In Section 5.3.3, results of method defined measures are presented. In Section 5.3.3.1, a comparison between the camera modules are presented.

All camera modules endured doses higher than the expected 300 Gy, yielding a sufficient amount of image snapshots. None of the modules froze (that is, sent the same picture more than once). Samples of the images are attached in Appendix B.

5.3.1 Assessment

The quality degradation is assessed in terms of the metrics described in Chapter 3. The metric algorithms were executed in MATLAB R2015b (version 8.6.0). All of the quality graphs are presented under Section 5.3.2.

5.3.1.1 PSNR & MSE

The assessment performed in terms of PSNR show a distinct initial degradation of image quality, followed by a like-wisely clear cumulative degradation. To avoid deception from the logarithm dB scale, the MSE values are also plotted and presented in Section 5.3.2.

Matlab Implementation The assessment was performed using the MATLAB Image Processing Toolbox implementation of the metric, see [Mat16d] and [Mat16c].

5.3.1.2 SSIM

Assessing the image quality degradation in terms of SSIM (using default settings) yielded obscure results, see gray curves in quality graphs. Although the results show a distinct initial degradation of severe grade, the results also shows that during certain dose intervals the quality degradation decreased. This is distinct in the graphs of Camera Module 3 and 4. Analyzing the statistics of cumulative degradation yields the mean and standard deviation values in Table 5.2. The statistics show less than 5/100 units in standard deviation, which equals less than 5% of the SSIM range (**[0..1]**). The SSIM did thus not show a substantial variation in cumulative degradation using default settings.

As the SSIM allows for adjustment, assessment was also performed with a 61x61 Gaussian window with standard deviation 10. The importance of luminance and contrast was increased to 3, whereas the structure importance remained unchanged. The adjusted settings yielded evident results showing a cumulative degradation of quality, see black curves in quality graphs.

	Camera Module			
	1	**2**	**3**	**4**
Mean	0.73	0.72	0.73	0.68
Std. dev.	0.03	0.05	0.03	0.04

Table 5.2: Result statistics of cumulative degradation using SSIM with default settings

Matlab Implementation Grayscale conversion and assessment was performed using the Matlab Image Processing Toolbox implementations, see [Mat16e] [Mat16a].

5.3.1.3 Improved CIELAB

Improved CIELAB shows distinct initial degradation followed by distinct cumulative degradation.

Matlab Implementation As Hassan does not provide an implementation of the metric, one was developed for Matlab, see Appendix C.

5.3.2 Quality graphs

Quality graphs are presented in Figure 5.9-5.24. Metric respective plotting windows are using the same vertical scales for convenient comparison between camera modules. The horizontal scales (absorbed dose) ranges from -10 Gy and upwards to explicitly visualize the initial degradation (when the irradiation commences). No universal upper bound is set on the horizontal axis since the modules endured substantially different doses. The upper bound is thus set to the value at which the camera module went completely out of operation (the image went black).

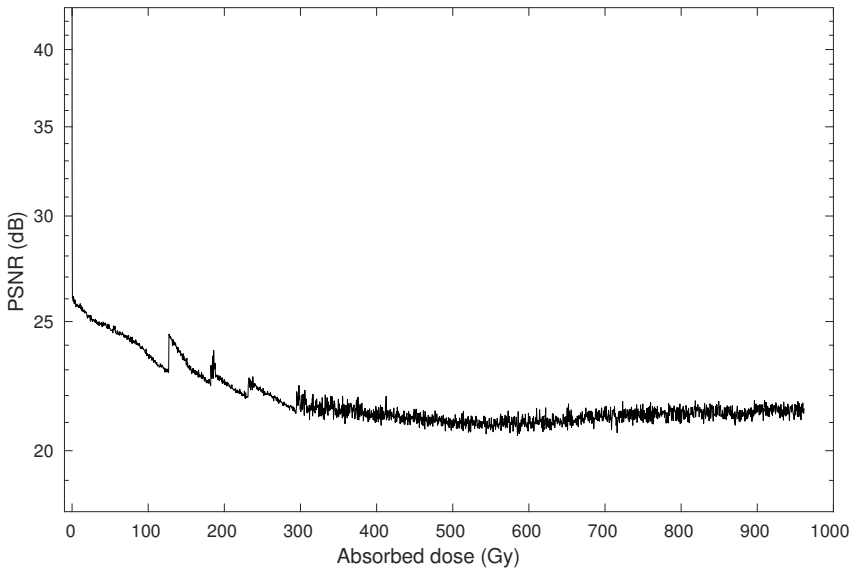

Figure 5.9: Camera Module 1: PSNR

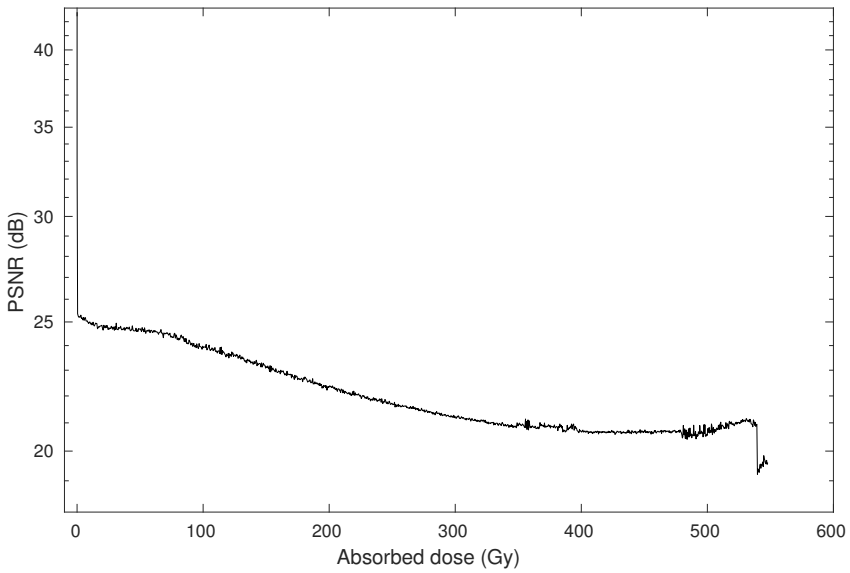

Figure 5.10: Camera Module 2: PSNR

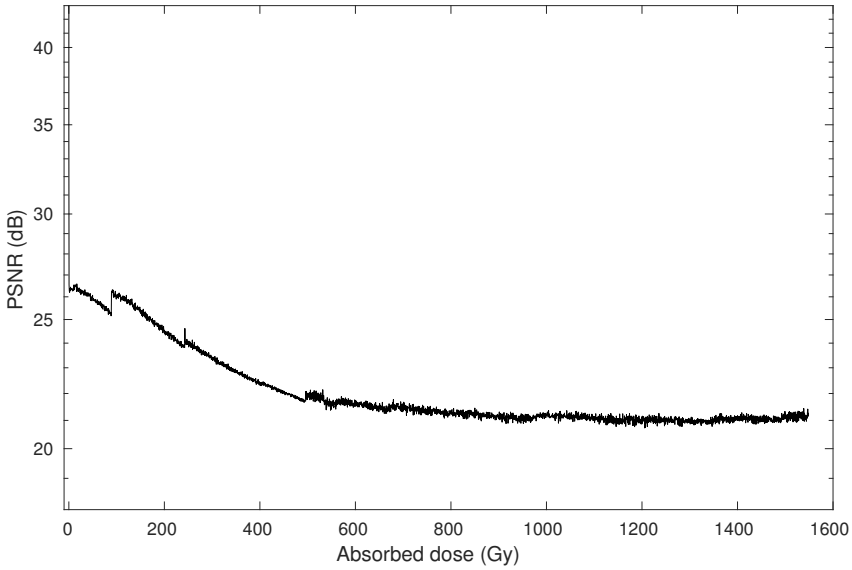

Figure 5.11: Camera Module 3: PSNR

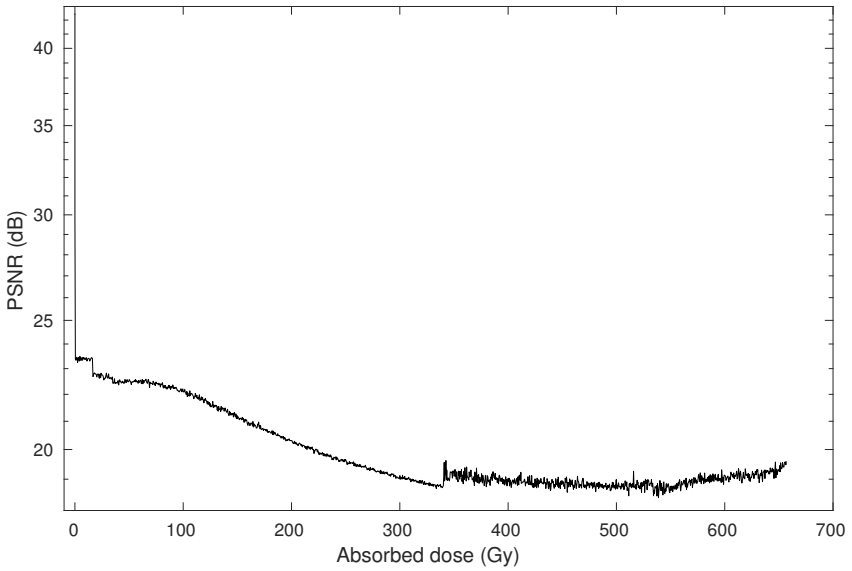

Figure 5.12: Camera Module 4: PSNR

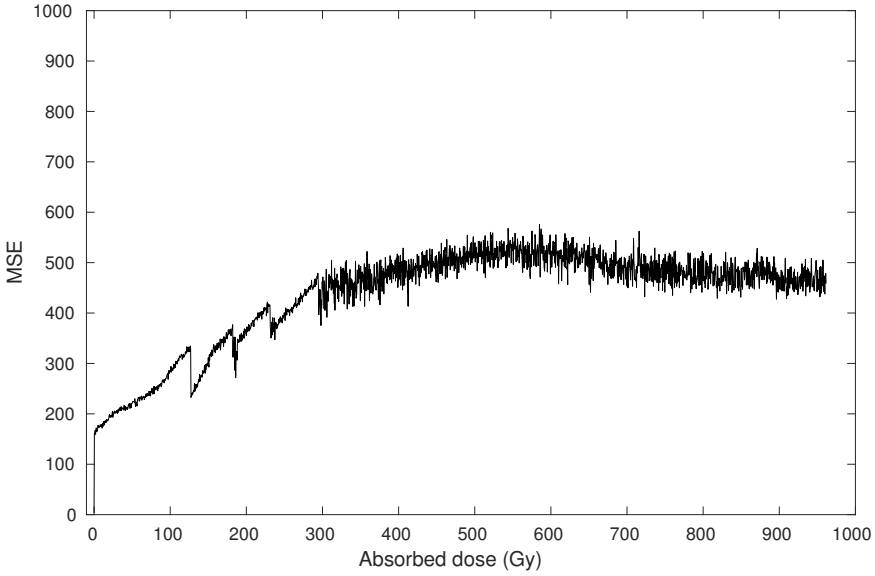

Figure 5.13: Camera Module 1: MSE

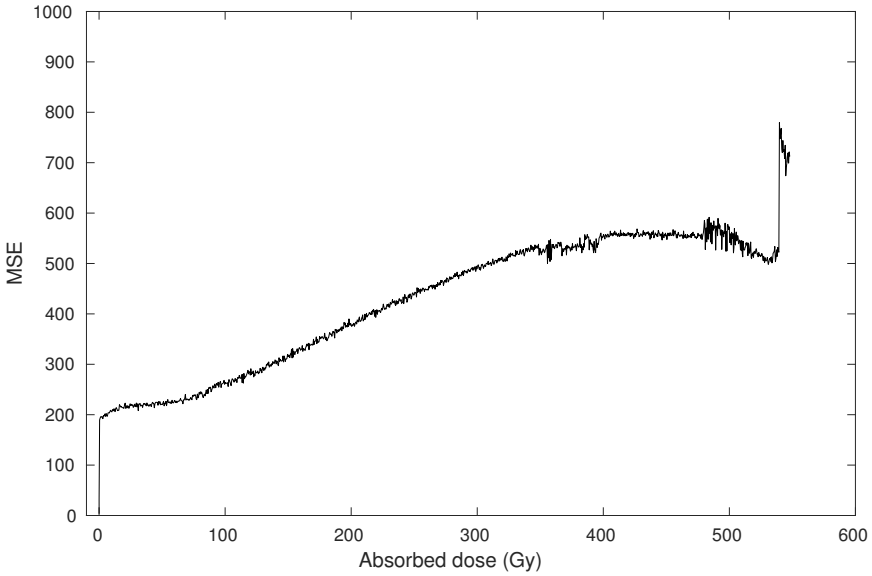

Figure 5.14: Camera Module 2: MSE

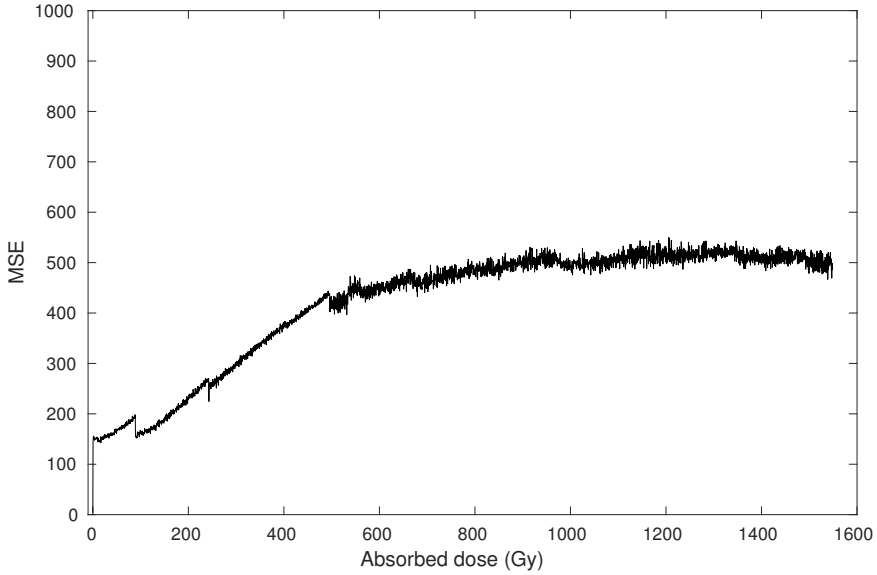

Figure 5.15: Camera Module 3: MSE

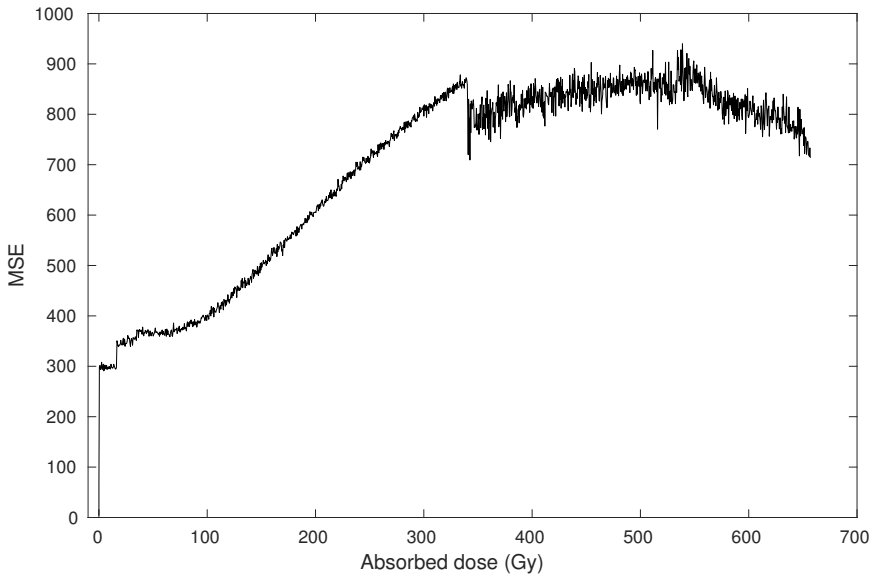

Figure 5.16: Camera Module 4: MSE

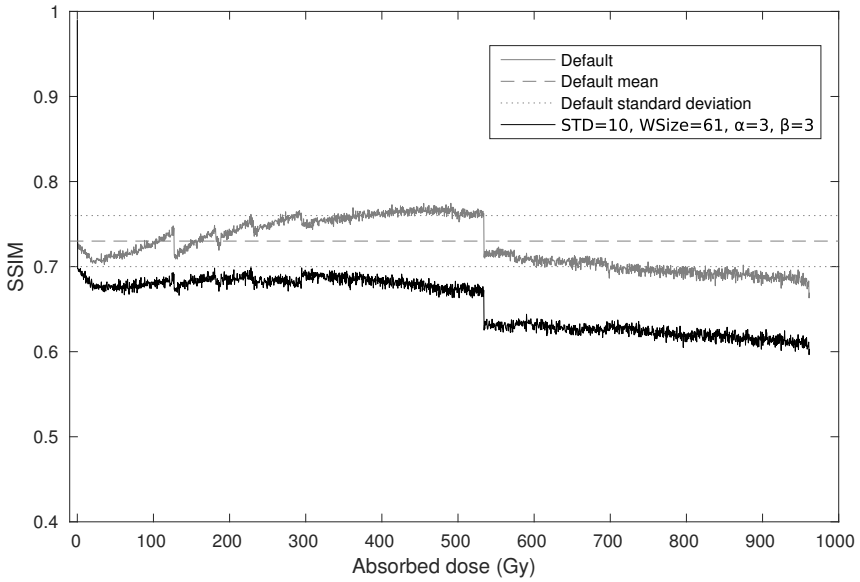

Figure 5.17: Camera Module 1: SSIM

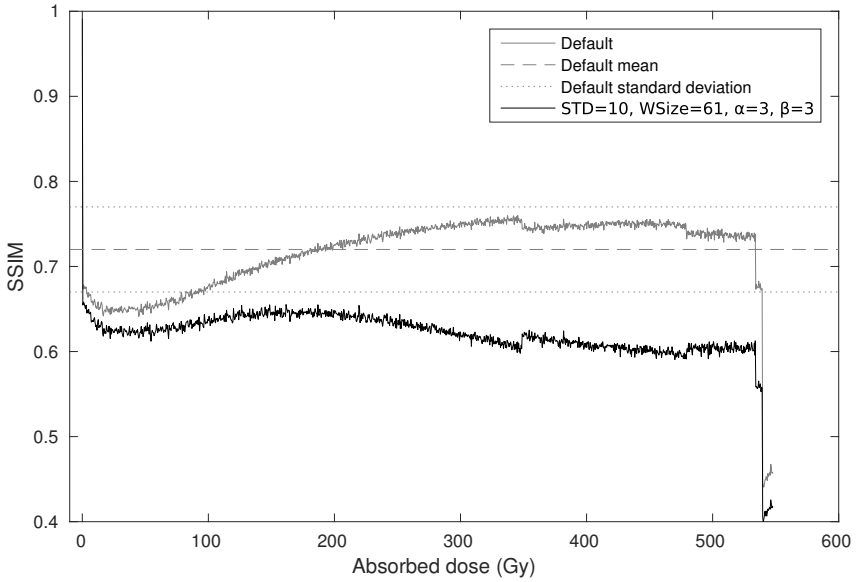

Figure 5.18: Camera Module 2: SSIM

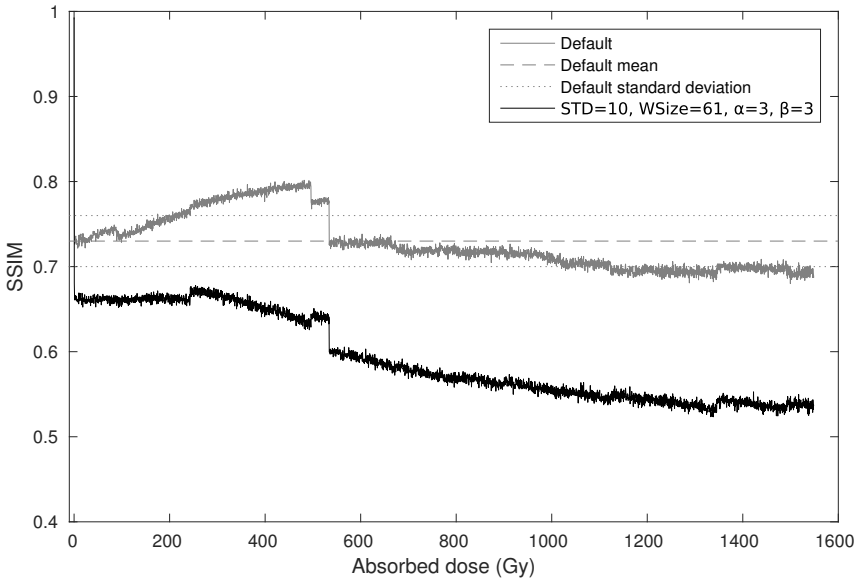

Figure 5.19: Camera Module 3: SSIM

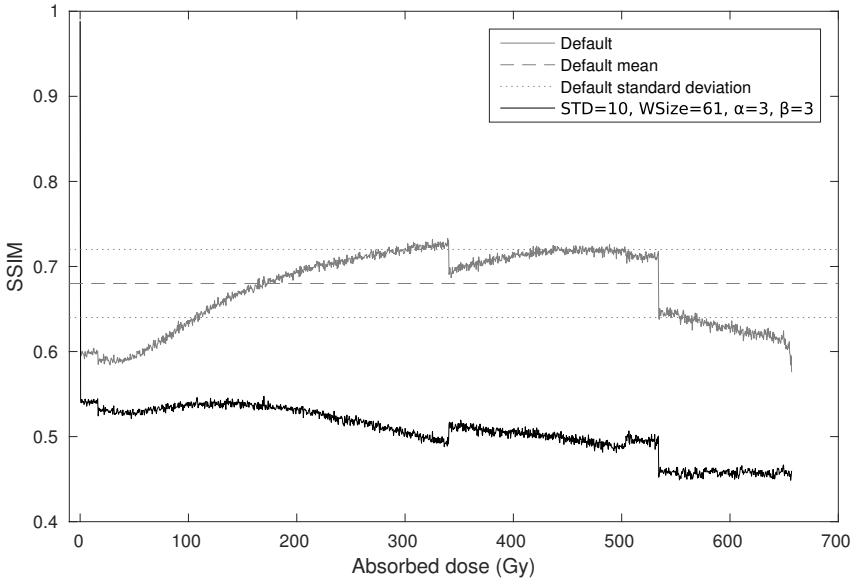

Figure 5.20: Camera Module 4: SSIM

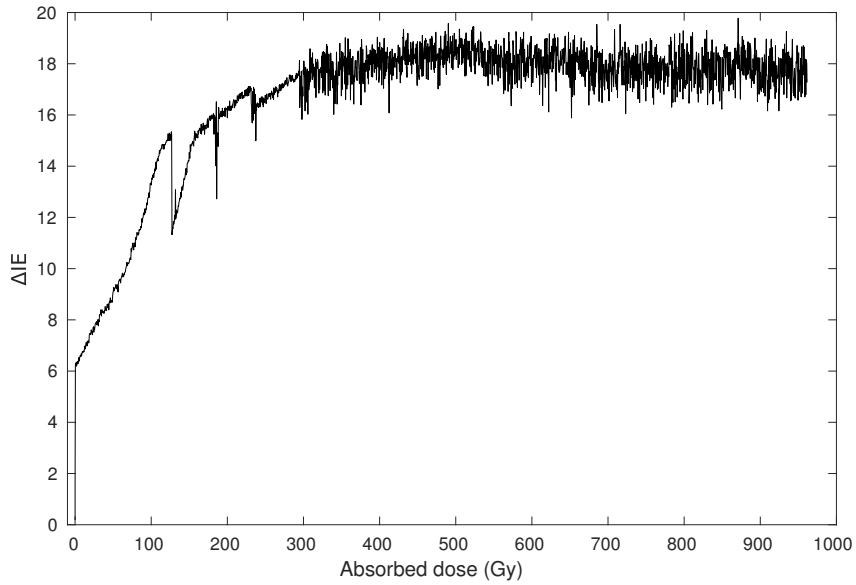

Figure 5.21: Camera Module 1: Improved CIELAB

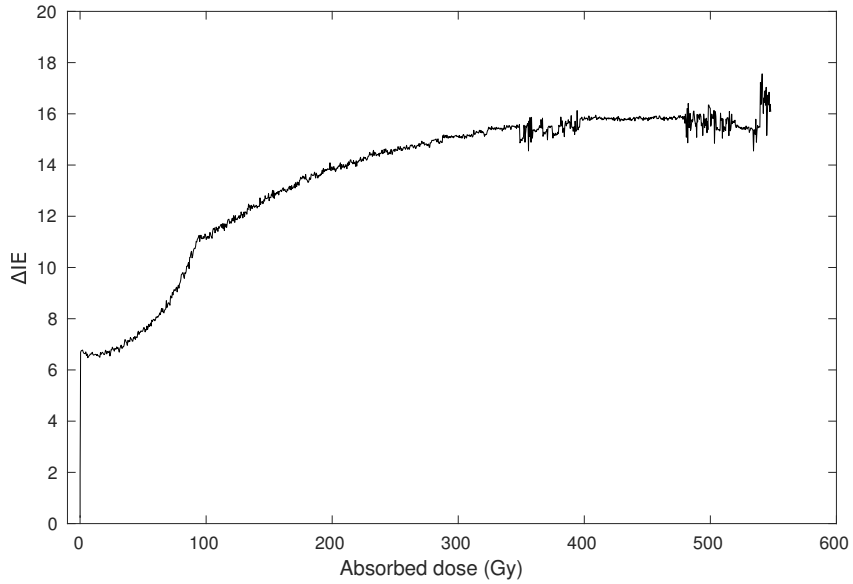

Figure 5.22: Camera Module 2: Improved CIELAB

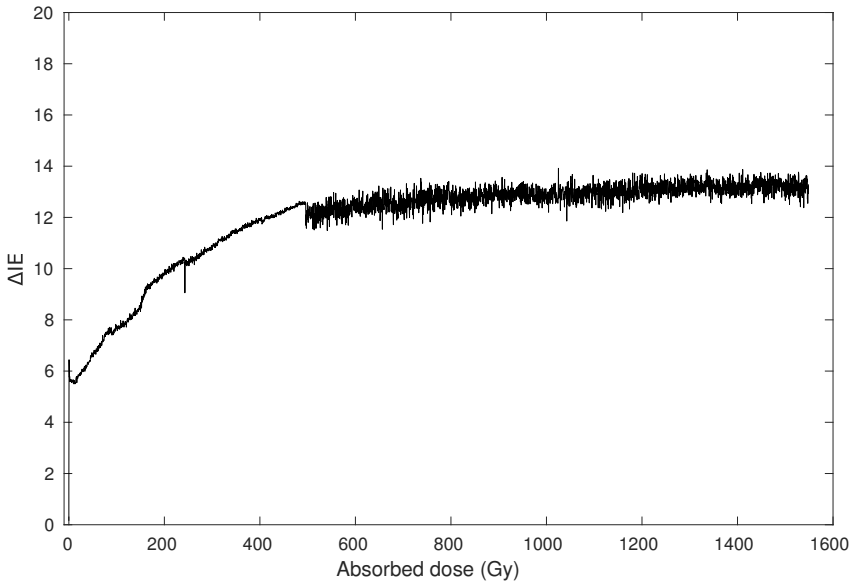

Figure 5.23: Camera Module 3: Improved CIELAB

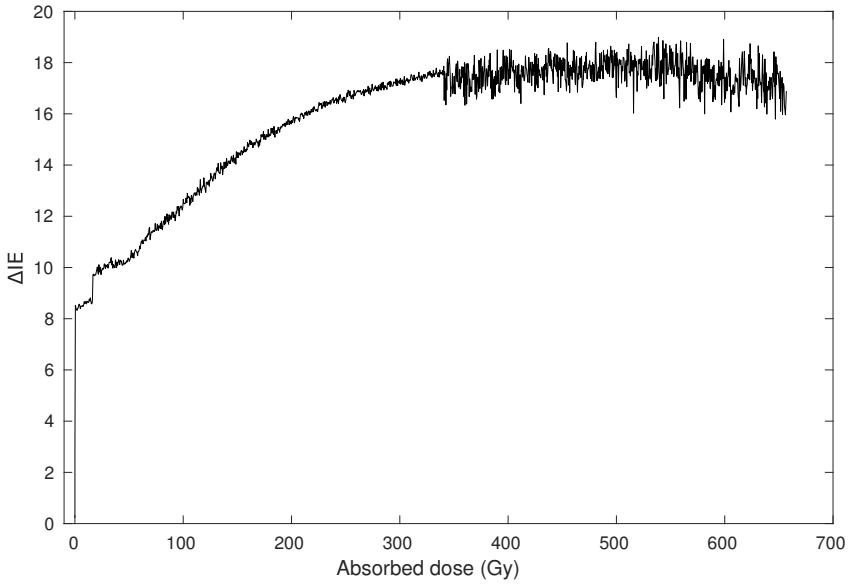

Figure 5.24: Camera Module 4: Improved CIELAB

5.3.3 Measurements

This section presents the results of the measures prescribed in the method. Total and cumulative degradation are measured by **500 Gy**, which is a dose level that all camera modules survived.

	Camera Module			
	1	**2**	**3**	**4**
Total dose (Gy)	962	548	**1549**	657

Higher is better.

Table 5.3: Dose endurance

	Camera Module			
	1	**2**	**3**	**4**
PSNR (dB)	26.0	25.4	**26.6**	23.4
SSIM (adjusted)	**0.7**	0.66	0.66	0.54
ΔIE	**6.26**	6.69	6.44	8.52

PSNR, SSIM: *Higher is better.*
ΔIE: *Lower is better.*

Table 5.4: Initial degradation

	Camera Module			
	1	**2**	**3**	**4**
PSNR (dB)	21.0	20.6	**21.9**	19.0
SSIM (adjusted)	**0.68**	0.61	0.64	0.49
ΔIE	18.7	16.2	**11.9**	16.6

PSNR, SSIM: *Higher is better.*
ΔIE: *Lower is better.*

Table 5.5: Total degradation by 500 Gy absorbed dose

	Camera Module			
	1	**2**	**3**	**4**
PSNR (dB)	5.0	4.8	4.7	**4.4**
SSIM (adjusted)	*0.02*	0.05	*0.02*	0.05
ΔIE	12.4	9.51	**5.46**	8.08

Lower difference is better
See Formula 4.1-4.2

Table 5.6: Cumulative degradation by 500 Gy absorbed dose

5.3.3.1 Result utilization

To demonstrate how the results can be utilized, we make an example in which we seek to determine which camera module that performed best under irradiation.

- Considering the dose level at which the camera modules were entirely defective it is clear that Camera Module 3 outperforms the other camera modules. See Table 5.3.
- Considering the *initial degradation*, Camera Module 3 performs best according to PSNR. Camera Module 1 performs slightly better than Camera Module 3 according to both SSIM (adjusted) and Improved CIELAB. See Table 5.4.
- Considering the *total degradation* by 500 Gy, Camera Module 3 performs best according to PSNR and Improved CIELAB, although Camera Module 1 performs best according to SSIM (adjusted). See Table 5.5.
- Considering the *cumulative degradation* by 500 Gy, Camera Module 4 performed best according to PSNR. Camera Module 1 and 3 performed equally in SSIM (adjusted), although Camera Module 3 performed best according to Improved CIELAB. See Table 5.6.

With the above considered results it is possible to determine which camera module performed best under irradiation. Giving the highest scoring camera module 1 point per result and metric (e.g. initial degradation: 2 points to Camera Module 1 and 1 point to Camera Module 3), ignoring relative difference, yields 3 points to Camera Module 1 and 5 points to Camera Module 3 (Cumulative SSIM, tie between Camera Module 1 and 3, result therefore discarded). Hence, **Camera Module 3 performed best.**

5.4 Chapter summary

This chapter has described an implementation of the proposed method on how to evaluate and quantify the effects that ionizing radiation has on image sensors. As IOE, the OV7949 was used in the context of a small camera module.

The chapter has described one approach to the methods first task (Gathering data). How to gather data (creating the image series) will obviously differ between different IOEs and different test environments. In the second task (Analysis), the execution of metric algorithms was performed in MATLAB R2015 with reason of convenient graph plotting features. However, other tools capable of the task would suit equally fine.

The quality degradation is assessed and expressed in relation to absorbed dose. The total degradation is visualized as plotted graphs. Three measurements are made: initial-, cumulative and total degradation. Considering the results, the best camera module is determined. The answer was distinctly Camera Module 3.

Assuming that image quality can only degrade and not improve during irradiation, the presented results prove the methods functionality. This is verified by all quality graphs, although SSIM (using default settings) remained relatively constant in *cumulative degradation* (as shown by statistics in Table 5.2).

The next chapter presents the conclusions drawn from this thesis and the proposed method. Presented is also openings for future work.

Chapter 6

Conclusions and Future Work

This thesis has proposed a method on how to evaluate and quantify the effects that ionizing radiation has on image sensors. Specifically, the method evaluates the effect from the perspective of image quality. Contrary to previous methods, the proposed possess a number of advantages:

- **Entirety:** The proposed method covers all the effects that are visible on image output and thus affects image quality. It is natural to discuss performance of image devices from the perspective of image quality, whereby non-visible radiation effects may be considered irrelevant.
- **Valuable and comparable:** Radiation effects are easier compared and valued when evaluated directly from the image quality perspective. With previous quantifications it was difficult to determine whether glass browning disturbs image quality more than dark current increase.
- **Hardware independence:** As the method operates on image quality, the method can be considered a black-box test where the only input interface is digital images. Hence, the method is applicable to anything that produces such images, whereby the evaluated object is referred to as Imager of Evaluation (IOE). This implies that effects induced in components surrounding the image sensor (optics, for example) are also taken into consideration. Automatic adjustment functions, such as gamma correction and white balance, are neither neglected. This contributes additionally to the method's *entirety* advantage.
- **Meaningful input:** Some of previous evaluations have been performed using input which is unrealistic in respect to image quality. One example is dark current which is naturally measured in a completely light-shielded environment.

The method has been demonstrated on four samples of one sensor model. Under the assumption that image quality should only degrade in relation to absorbed dose, the results of the demonstration verifies the method's functionality.

Demonstrated was also an example of how the results from the evaluation can be utilized. The example was to determine which sample that performed best under irradiation.

6.1 Application

The work of this thesis can be of certain interest among manufacturers of radiation tolerant cameras, specifically within the purpose of verifying radiation tolerance. One example is to determine a threshold of which the image quality is so degraded that the IOE can be considered defective, and thus decide whether warranty will be granted or not. As of today, data sheets of most manufacturers only present a value of absorbed dose that their cameras are guaranteed to withstand [Dia] [Mir]. Image quality degradation is not taken into consideration. Refining the proposed method could imply new approaches to verifying radiation tolerance. In the best of scenarios, such pursuit would entail a new industrial standard of verification in which image quality is taken into account.

It is also possible to define additional measures of image quality degradation. One example is to consider the derivative of in order to answer how fast image quality degrades in respect to absorbed dose. Such measures can be sincerely interesting when comparing radiation performance among IOEs.

6.2 Future work

Openings for future work lies primarily within two fields: metrics and method verification.

The results of the demonstration experiment stated that the Improved CIELAB and PSNR metrics showed a significant cumulative degradation. However, SSIM (default) remained relatively constant when dose was absorbed (see statistics in Table 5.2). One must not be deceived by this and conclude that SSIM is a metric that does not measure the effects caused by ionizing radation. SSIM is sensitive to image structure (among other quality factors) [WBSS04]. Looking at the image series it is clear that the structure was not substantially altered after irradiation start. As the metrics show distinctly different results, there clearly needs more work on finding one or a set of metrics that best resemble the human visual systems perception of the effects that ionizing radiation induces on image quality. The proposed method relies on image quality assessment rather than certain metrics, whereby the metrics could be replaced if better ones are found. Investigating metrics correlation to human visual perception is normally performed by comparing metric's assessment with some subjective assessment method (Mean Opinion Score, for example). Subjective assessment is known for being inaccurate when performed with few subjects. Investigation requires therefore many subjects, implying a time-consuming and expensive process.

More work needs also to be done in effort to verify the methods functionality. Such work is also time-consuming and costly whereby the demonstration experiment performed in this thesis was restricted to one sensor model only. Restricted was also the irradiation test conducted as part of the experiment. Aspects of irradiation restriction is listed below:

- One radiation type: Gamma photons from ^{235}U
- One dose rate: 30 Gy/h
- One session - how would pauses of irradiation affect the image quality degradation?

Appendix A

Introduction to Image Sensors

Image sensors are diverse components, coming in many forms and in different implementations. The aim of this chapter is to provide a **brief** introduction to the construction concepts and operational characteristics of two image sensors: CMOS and CCD.

The approach goes from the bottom and upwards. Section A.1 describes photodetectors. Photodetectors are the smallest and most elementary part of the image sensor. Each pixel employs a photodetector, which is responsible for converting photons to electrical signals. Section A.2 describes the CCD and the CMOS image sensors. How to introduce colors in otherwise monochrome image sensors are described in Section A.3.

A.1 Photo detectors

Rasterized images are matrices of pixels, whereas pixels are the smallest distinguishable areas of an image [Gra99]. In an image sensor, pixels employ several electric components, although the most essential component is the photodetector. Photodetectors are responsible for fulfilling the main purpose of the image sensor pixel, that is, to convert light into an electric signal. The electrical signals from the pixel matrix are combined to assemble an electronic picture.

Different types of photo detectors are used in different types of image sensors. In this chapter, two types of photo detectors are reviewed. Those are *photogates* and *photodiodes*. Photogates are strongly related to the CCD sensor, as they originate from the same invention. Photodiodes can be found in many other light-dependent applications, such as solar cells, opto-couplers, security sensors and industrial applications [Pal07]. Both photodiodes and photogates have in common that their function relies on the photo-electric effect in semiconductor materials.

A.1.1 Photodiode

The photodiode may be implemented using a *p-n* junction (other implementations exist as well, see [FH+14b]). In short, a semiconductor junction is a boundary between two doped semiconductor materials. In a p-n junction, the materials are p- and n-doped respectively. The n-doped substrate is referred to as *cathode* and is rich on free electrons. The other end, the p-doped substrate, is referred to as *anode* and is rich on electron holes [TS11].

Semiconductor junctions are sensitive to light according to the photoelectric effect. If a photon with sufficient energy (that is, energy greater than the substrate's bandgap, e.g. 1.166 eV for Si) strikes the junction, electrons in the valence band may be liberated and moved to the conduction band. This gives rise to a flow of electrons to the n-region and of holes flowing to the p-region, that is, between the anode and the cathode. This is called a *photocurrent* [TS11]. Due to thermally generated diffusion a flow may occur in the diode, even if not being exposed to light. This is defined as the *dark current* [TS11].

The measurement of generated electron-hole pairs per incident photon is measured by the *quantum efficiency* quotient, defined as

$$\eta = \frac{N_e}{N_v} \tag{A.1}$$

where N_e and N_v denotes number of electrons produced and number of photons absorbed respectively.

Using a p-n junction as photodetector was proposed by Weckler in 1967 [Wec67]. Since then, photodiodes have been widely used in different opto-applications, such as scanners, fiber-optic receivers and solar cells [Gra99].

A.1.2 Photogate

The photogate is, in short, a MOS structure capacitor. Most simplified, the photogate converts light to *electric charge*. The structure consists of an silicon dioxide film that is sandwiched between a metal plate (called the gate) and a p-n junction [Tay98].

When photons with sufficient energy enters the photogate, electron-hole pairs may be created as a result of the photoelectric effect. If a voltage is applied on to the gate, the electrons will drift to the n-type silicon where they are trapped. This gives rise to charge accumulation. Removing the applied voltage allows for transferring the charge from the photogate, whereby it can be amplified to an output signal [Tay98].

A.2 Sensor types

This section describes two types of image sensors types: CMOS and CCD. Described are their basic operation characteristics and fundamental differences. Sensor types differ in many traditional performance aspects. The performance differences between CMOS and CCD are well reviewed by Litwiller and Bigas et al [Lit01] [BCFS06].

Section A.1 has described two major approaches to convert light into electric signals. Different image sensors are implemented using different photodetectors. Except for the photodetection mechanisms, image sensors can also be divided into two groups, depending on readout approach. CCDs are defined as *charge transfer* image sensors, further described in Subsection A.2.2. Contrary to charge transfer, CMOS uses an X-Y addressable approach.

Figure A.1 provides a comprehensive overview of the relations between CCD- and CMOS image sensors, their addressing and photosensing mechanism.

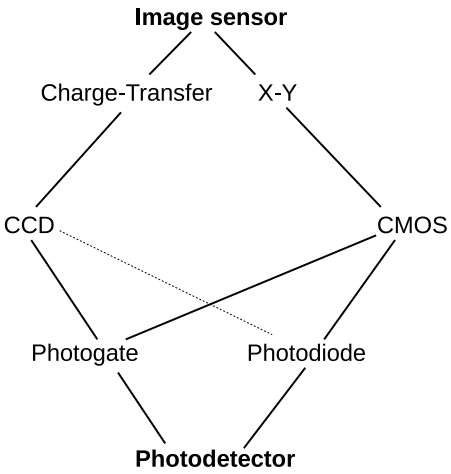

Figure A.1: Image sensors overview

A.2.1 CMOS: Complementary Metal-Oxide-Semiconductor

As Figure A.1 shows, CMOS sensors are most often implemented using photodiodes, but implementations based on photogates exist as well [FH14a] [Pal07].

Figure A.1 also shows that CMOS sensors are of X-Y addressed readout. In short, X-Y addressed readout means that each pixel is individually accessed. Addressing is realized using column- and row multiplexers by the edges of the pixel matrix [Lit01] [Nak06]. Simple control electronics can thus be used to retrieve the values from each pixel and send them to the next step in the signal chain. This

concept of addressing is general for CMOS sensors, but the readout process and operation differs between three architectures; the Passive Pixel Sensor, the Active Pixel Sensor and the Digital Pixel Sensor. Their differences are briefly described in the list below.

CMOS PPS In the CMOS Passive Pixel Sensor, photodetectors signal outputs are amplified by a common amplifier.

CMOS APS In the CMOS Active Pixel Sensor, amplifiers reside in every pixel, hence the name.

CMOS DPS In the CMOS Digital Pixel Sensor, both amplifiers and ADC's reside in every pixel.

The background of the X-Y addressing approach lies in the integration potential of the CMOS manufacturing process. The process allows for additional CMOS components to be put onto the same chip, for example, signal processing elements. This concept is sometimes referred to as Camera-on-Chip, and is reviewed in great manner by Fossum [Fos97]. However, the major drawback of putting more components in **each pixel** is the reduced *fill factor*. The fill factor measure the density of the pixels in the image sensor - lower fill factor leads to lower sensitivity [BCFS06].

A.2.2 CCD: Charge-Coupled Device

When the CCD was being developed by Willard Boyle and George Smith at the AT&T Bell Labs in 1969, it was initially intended to be a computer memory [WG74] [Tay98]. Soon after its invention, it was clear that the MOS capacitors were light-sensitive according the the photoelectric effect. The memory's contents changed when being exposed to light [Tay98]. Upon this discovery, Smith was quoted saying: *"(we) invented charged-coupled devices in an hour"* [Tay98]. The discovery of the photo electric effect in the CCD lead to first patent of CCD as an image sensor in 1972 is held by M.F. Tompsett [Tom78].

The memory was constructed using a matrix of MOS capacitors, where the capacitors would serve as memory cells. From here, we use the term photogate instead of MOS capacitor to explicate that the CCD is described in form of an image sensor.

As depicted in Figure A.1, the CCD is of charge-transfer readout architecture. By applying voltage to a photogate, charge accumulation from incident light is enabled. If applying voltage to its adjacent photogate and removing the voltage from the first one, the charge can be moved to the adjacent photogate. The process has similarities with the readout of a shift register [Tay98] [Nak06]. Although the charge transfer mechanism is general for CCD's, the readout process differs between CCD architectures. Three readout methods are described in Section A.2.2.1.

As Figure A.1 states, the CCD image sensor is primarily implemented using photogates. Although implementations using pinned photodiodes exist as well [FH14a] [Bla01].

A.2.2.1 Readout methodologies

Full Frame Readout One approach to pixel readout is to transfer charges of all photogates of one matrix row to the next row in the matrix, and thus move rows towards the matrix' edge. On the edge, a special row is used to transfer individual columns of that row (that is, individual buckets) towards a charge amplification unit, preceded by the control electronics [Tay98] [Lit01]. This sequential approach is normally called *full frame readout* and is sometimes also referred to as the rain-bucket principle [How99]. Figure A.2 describes the full frame readout process.

The full frame readout process is operating directly on the photogate matrix, which poses certain consequences. One of these consequences are that photogates are still being exposed to light during the read out process of the desired snapshot. If the light changes, so does the picture. This phenomena is often called *rolling shutter*. To encounter this problem, mechanical shutters can be used, but other readout approaches exist as well [Tay98] [Jun98].

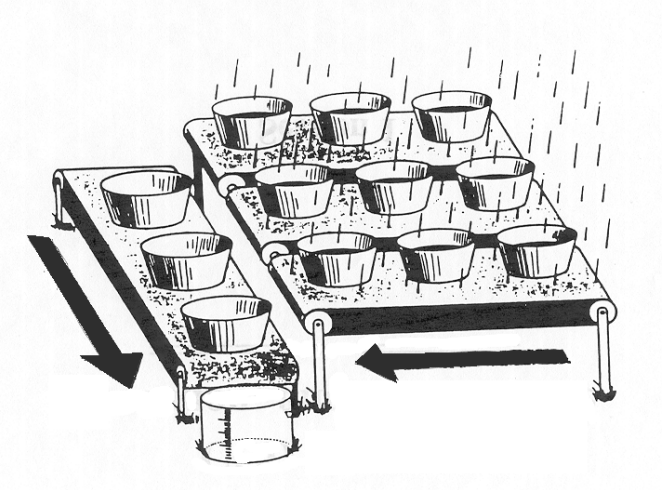

Figure A.2: CCD Full Frame readout
The Rain-bucket principle
From [How99]

Frame transfer readout To encounter the problems of full frame readout, the *frame transfer readout* method is an alternative. The principle is essentially the same as full frame readout, but to countermeasure the problem, the

photogate charges are *transferred* to a second light-shielded 'photogate' matrix. Further on, the shielded matrix is read out according to the full frame readout method [Tay98] [Jun98]. Obviously, this readout method takes substantially longer time.

Split frame transfer readout To minimize the readout time in the frame transfer method, several compromises exist. One is the *split frame transfer*, which is essentially the same as the frame transfer method. The difference is that the shielded matrix has been divided in two parts - one part located above the non-shielded matrix and one below. This reduces the readout time by factor of two [Tay98].

A.3 Color filtering

Image sensors and photodetectors are monochrome devices, responding to light energies only. To introduce colors in image sensors, a method is needed to separate the light in different wavelengths. This is accomplished by a *color filter*.

Color filters are, essentially, matrix patterned LP, BP and HP filters put in front of the image sensor. The most commonly used color filter is the *Bayer filter*. The Bayer filter fusions four monochrome photodetectors into one color pixel. Each photodetector is filtered and decoded as a certain color. The Bayer-filter features two green photodetectors, one red and one blue [Nak06]. Four monochrome photodetectors fusioned to a color pixel by a Bayer filter is depicted in Figure A.3.

The drawback is, naturally, lower resolution as each color pixel requires four physical photodetectors.

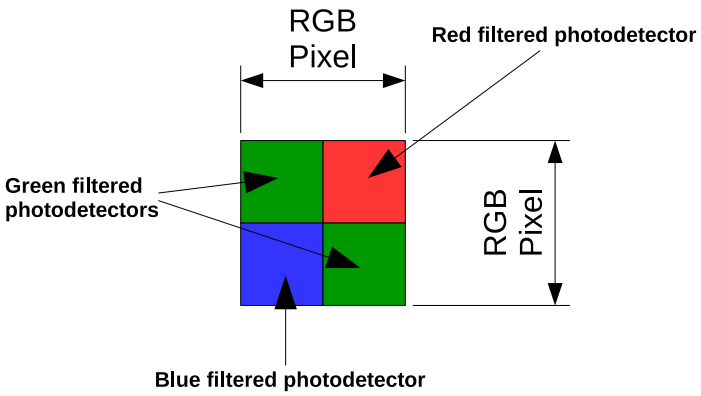

Figure A.3: Bayer color filtered pixel

Appendix B

Image Series

In this appendix, three images captured by the experiment IOE (Chapter 5) are attached.

The three images are taken:

1. Before irradiation: Shows the original image quality.
2. Beginning of irradiation: Shows initial quality degradation.
3. End of irradiation: Shows total quality degradation.

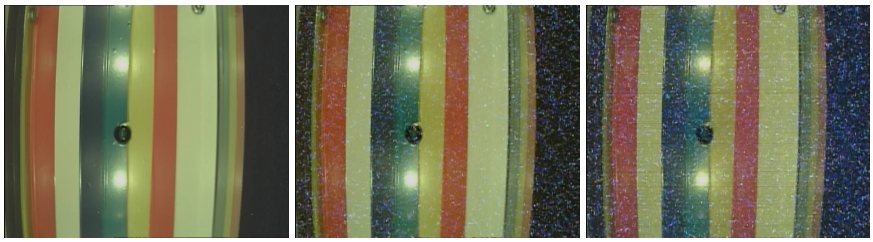

Figure B.1: Camera Module 1: Taken at 0, 1.5 and 962 Gy

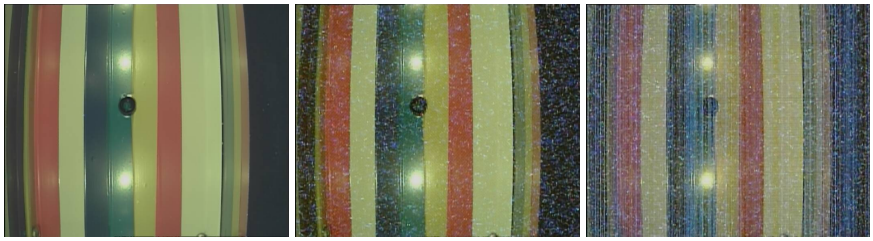

Figure B.2: Camera Module 2: Taken at 0, 1.5 and 548 Gy

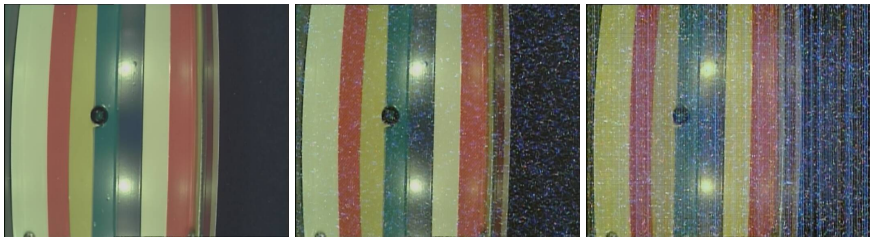

Figure B.3: Camera Module 3: Taken at 0, 1.5 and 1549 Gy

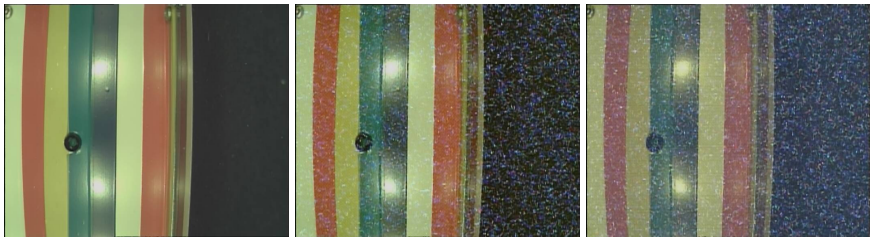

Figure B.4: Camera Module 4: Taken at 0, 1.5 and 657 Gy

Appendix C

Improved CIELAB Matlab Implementation

As Hassan [Has15] does not provide an implementaiton of the Improved CIELAB metric, one was written for Matlab.

The implementation uses the Matlab Image Processing Toolbox's RGB-to-CIELAB conversion function, which converts to CIELAB using the D65 whitepoint [Mat16b].

Listing C.1: Improved CIELAB (ΔIE) Matlab Implementation

```
function dIE_value = dIE(img1, img2)

img1 = rgb2lab(img1);
img2 = rgb2lab(img2);
dE_sum = 0;

for x = 1:length(img1(1,:,1))
  for y = 1:length(img1(:,1,1))
    pixel1 = permute(img1(y,x,:),[3 1 2]);
    pixel2 = permute(img2(y,x,:),[3 1 2]);
    dE_pixel = norm(pixel1-pixel2);
    if dE_pixel > 2.3
      dE_sum = dE_sum + dE_pixel;
    end
  end
end

dIE_value = dE_sum/double(numel(img1(:,:,1)));

return;
```

References

[Axi13] Axis Communications AB. *VAPIX API, version 3: Video Streaming API*, m4.2 edition, July 2013.

[BCFS06] M Bigas, Enric Cabruja, Josep Forest, and Joaquim Salvi. Review of CMOS image sensors. *Microelectronics journal*, 37(5):433–451, 2006.

[BD00] Jan Bogaert and Bart Dierickx. Total dose effects on CMOS active pixel sensors. In *Sensors and Camera Systems for Scientific, Industrial, and Digital Photography Applications*, volume 3965, pages 157–167, 2000.

[BDMU03] J. Bogaerts, B. Dierickx, G. Meynants, and D. Uwaerts. Total dose and displacement damage effects in a radiation-hardened CMOS APS. *IEEE Transactions on Electron Devices*, 50(1):84–90, Jan 2003.

[Bis70] Adli Bishay. Radiation induced color centers in multicomponent glasses. *Journal of Non-Crystalline Solids*, 3(1):54–114, 1970.

[Bla01] Nicolas Blanc. CCD versus CMOS – has CCD imaging come to an end?, 2001. Wichmann Verlag, Heidelberg.

[BN98] Hans Bach and Norbert Neuroth, editors. *The Properties of Optical Glass*. Schott Series on Glass and Glass Ceramics. Springer-Verlag Berlin Heidelberg, 1 edition, 1998.

[Con] Conrad Elektronik Norden AB. Conrad OEM RS-OV7949-1818 Specification. `http://www.produktinfo.conrad.com/datenblaetter/150000-174999/156967-da-01-en-FARB_KAMERA_MODUL_RS_OV7949_1818.pdf`.

[Cur] Robert A. Curtis. Introduction to ionizing radiation. United States Government, Department of Labor, Occupational Safety and Health Administration, `https://www.osha.gov/SLTC/radiationionizing/introtoionizing/ionizinghandout.html`. Accessed: 2016-04-27.

[Dia] Diakont Advanced Technologies. Cctv camera solutions spec sheet. http://www.diakont.com/wp-content/uploads/2011/08/DIAK-Product-D70_03-0601-07.pdf. Accessed: 2016-05-13.

[Dom10] Public Domain. Camera obscura. https://commons.wikimedia.org/wiki/File:Camera_obscura_1.jpg, 1910.

[EAF02] E. S. Eid, S. U. Ay, and E. R. Fossum. Design of radiation tolerant CMOS APS system-on-a-chip image sensors. In *Aerospace Conference Proceedings, 2002. IEEE*, volume 4, pages 4–2005–4–2011 vol.4, 2002.

[EDASE08] L.M. Sharaf El-Deen, M.S. Al-Salhi, and M.M. Elkholy. Radiation induced color centers in 50pbo–50p2o5 glass. *Journal of Non-Crystalline Solids*, 354(52–54):5453 – 5458, 2008.

[FH14a] E.R. Fossum and D.B. Hondongwa. A Review of the Pinned Photodiode for CCD and CMOS Image Sensors. *Electron Devices Society, IEEE Journal of the*, 2(3):33–43, May 2014.

[FH+14b] Eric R Fossum, Donald B Hondongwa, et al. A review of the pinned photodiode for ccd and cmos image sensors. *IEEE J. Electron Devices Soc*, 2(3):33–43, 2014.

[Fos97] E. R. Fossum. CMOS image sensors: electronic camera-on-a-chip. *IEEE Transactions on Electron Devices*, 44(10):1689–1698, Oct 1997.

[Gir93] Bernd Girod. What's wrong with mean-squared error? In *Digital images and human vision*, pages 207–220. MIT press, 1993.

[GK12] Michał Gumiela and Rafał Kozik. Studies of the applicability of cmos and ccd sensors for detection, dosimetry and imaging of alpha, beta, gamma, x-ray and proton beam spots, 2012.

[Gra99] Rudolf F. Graf. *Modern Dictionary of Electronics*. Oxford: Newnes, 1999. ISBN 0-7506-4331-5.

[H+00] Gordon R Hopkinson et al. Radiation effects in a CMOS active pixel sensor. *IEEE Transactions on Nuclear Science*, 47(6):2480–2484, 2000.

[Ham81] J. H. Hammond. *The camera obscura: a chronicle*. CRC Press, 1981.

[Has15] Mohammed Ahmed Hassan. Perceived quality assessment of color images. *International Journal of Engineering Research and Technology*, 4(5):1592–1595, May 2015.

[HB12] Mohammed Hassan and Chakravarthy Bhagvati. Structural similarity measure for color images. *International Journal of Computer Applications*, 43(14):7–12, 2012.

[How99] Steve B. Howell. Basics of Charge Coupled Devices, 1999. National Optical Astronomy Observatory.

[HSA93] A. Holmes-Siedle and L. Adams. *Handbook of radiation effects*. Oxford science publications. Oxford University Press, 1993.

[HZ10] A. Hore and D. Ziou. Image Quality Metrics: PSNR vs. SSIM. In *Pattern Recognition (ICPR), 2010 20th International Conference on*, pages 2366–2369, Aug 2010.

[Jun98] R Jung. Image sensor technology for beam instrumentation. In *AIP Conference Proceedings*, pages 74–94. Citeseer, 1998.

[Lit01] Dave Litwiller. CCD vs. CMOS: Facts and Fiction. *Photonics Spectra*, 35(1):154–158, 2001.

[Mat16a] MathWorks Nordic. MATLAB rgb2gray. `http://se.mathworks.com/help/matlab/ref/rgb2gray.html`, 2016. Accessed: 2016-04-20.

[Mat16b] MathWorks Nordic. MATLAB rgb2lab. `http://se.mathworks.com/help/images/ref/rgb2lab.html`, 2016. Accessed: 2016-04-20.

[Mat16c] MathWorks Nordic. Mean-squared error - MATLAB immse. `http://se.mathworks.com/help/images/ref/immse.html`, 2016. Accessed: 2016-04-20.

[Mat16d] MathWorks Nordic. Peak Signal-to-Noise Ratio (PSNR) - MATLAB psnr. `http://se.mathworks.com/help/images/ref/psnr.html`, 2016. Accessed: 2016-04-20.

[Mat16e] MathWorks Nordic. Structural Similarity Index (SSIM) - MATLAB ssim. `http://se.mathworks.com/help/images/ref/ssim.html`, 2016. Accessed: 2016-04-20.

[MEO94] Marc Mahy, L Eycken, and André Oosterlinck. Evaluation of uniform color spaces developed after the adoption of CIELAB and CIELUV. *Color Research & Application*, 19(2):105–121, 1994.

[Mir] Mirion Technologies, Inc. RC710 Data sheet. `https://mirion.app.box.com/s/fekx2t83ch4kljrfb43g`. Accessed: 2016-05-13.

[MRLP+] M Martinez-Rach, O López, P Piñol, MP Malumbres, and J Oliver. PSNR vs. quality assessment metrics for image and video codec performance evaluation.

[Nak06] Junichi Nakamura. *Image sensors and signal processing for digital still cameras*. CRC Press, Taylor & Francis Group, LLC, 2006.

[Omn09] OmniVision Technologies Inc. OmniVision OV7949 Product Brief. `http://www.ovt.com/uploads/parts/OV7949_PB_%281.31%29.pdf`, August 2009. Accessed: 2016-04-27.

[Pal07] Atmaram Palakodety. CMOS Active Pixel Sensors for Digital Cameras: Current state-of-the-art. Master's thesis, University of North Texas, May 2007.

[Tay98] Stuart A. Taylor. CCD and CMOS Imaging Array Technologies: Technology Review, 1998.

[Tom78] M.F. Tompsett. Charge transfer imaging devices, April 18 1978. US Patent 4,085,456.

[TS11] Filip Tavernier and Michiel Steyaert. *High-Speed Optical Receivers with Integrated Photodiode in Nanoscale CMOS.* Analog Circuits and Signal Processing: 5. New York, NY : Springer New York, 2011., 2011.

[Vel16] Velleman Projects. *Velleman VM204 User Manual*, December 2016. `https://www.velleman.eu/downloads/0/user/usermanual_vm204_en.pdf`, Accessed: 2016-04-17.

[WBL02] Z. Wang, A. C. Bovik, and L. Lu. Why is image quality assessment so difficult? In *Acoustics, Speech, and Signal Processing (ICASSP), 2002 IEEE International Conference on*, volume 4, pages IV–3313–IV–3316, May 2002.

[WBSS04] Zhou Wang, A. C. Bovik, H. R. Sheikh, and E. P. Simoncelli. Image quality assessment: from error visibility to structural similarity. *IEEE Transactions on Image Processing*, 13(4):600–612, April 2004. Source code at `https://ece.uwaterloo.ca/~z70wang/research/ssim/index.html`.

[Wec67] G.P. Weckler. Operation of p-n Junction Photodetectors in a Photon Flux Integrating Mode. *Solid-State Circuits, IEEE Journal of*, 2(3):65–73, Sep 1967.

[WG74] B. W and S. G. Three dimensional charge coupled devices, March 12 1974. US Patent 3,796,927.

[WSB03] Z. Wang, E. P. Simoncelli, and A. C. Bovik. Multiscale structural similarity for image quality assessment. In *Signals, Systems and Computers, 2004. Conference Record of the Thirty-Seventh Asilomar Conference on*, volume 2, pages 1398–1402 Vol.2, Nov 2003.